Stony Brook University

Processing and Characterization of Chitosan and Hydroxyapatite filled Polymer Composites

A Thesis Presented

by

Karl Anthony Nelson

The Graduate School

in Partial Fulfillment of the

Requirements

for the Degree of

Master of Science

in

Mechanical Engineering

Stony Brook University

December 2009

Stony Brook University

The Graduate School

Karl Anthony Nelson

We, the thesis committee for the above candidate for the

Master of Science degree,

hereby recommend acceptance of this thesis.

Dr. Chad Korach, Advisor, Mechanical Engineering

Dr. Imin Kao, Chair, Mechanical Engineering

Dr. Gary Halada, Member, Materials Science and Engineering

This thesis is accepted by the Graduate School

Lawrence Martin
Dean of the Graduate School

Abstract of the Thesis

Processing and Characterization of Chitosan and Hydroxyapatite filled Polymer Composites

by

Karl Anthony Nelson

Master of Science

in

Mechanical Engineering

Stony Brook University

2009

Engineered biocompatible composites are gaining widespread use in the field of orthopedics. Biocomposites are developed to take advantage of the biological and mechanical properties of both phases to create better performance *in vivo*. These composite materials include chitosan-hydroxyapatite composites for use in bone cement and tissue scaffolding and polyethylene-hydroxyapatite composites for use in hip arthroplasty. The need exists to further develop the materials for improved strength and wear life.

Chitosan/hydroxyapatite composites were prepared and characterized to investigate bond strength and chemical interaction. Chitosan/hydroxyapatite

biocomposites were prepared by kneading a hydroxyapatite powder into a chitosan/malic acid gel. Hydroxyapatite varied from 86% w_f to 93% w_f. Malic acid was varied from 2% w_f to 7% w_f. Microstructure and bond strength were qualitatively measured using SEM, showing strong bonding between chitosan and hydroxyapatite. Raman spectroscopy showed a shift in the PO_4 peaks between neat hydroxyapatite and chitosan/hydroxyapatite composites, suggesting a change in bond structure at the filler-matrix interface. Atomic Force Acoustic Microscopy was used to analyze the elastic modulus of an individual hydroxyapatite particle coated with chitosan thin film, showing a decrease in elastic modulus from 70 to 10 GPa compared with virgin hydroxyapatite. These results indicate the use of a chitosan interlayer can improve bonding between hydroxyapatite fillers and a polymer matrix.

Ultra High Molecular Weight Polyethylene composites were prepared and characterized to investigate the bond strength and wear resistance. Hydroxyapatite and chitosan/hydroxyapatite composite fillers were used to reinforce hydroxyapatite at 5, 10 and 15% v_f. The composite were processed by dry mixing and hot pressing. SEM imaging showed an improvement in reinforcement-matrix bonding with the incorporation of a chitosan interlayer. A ball on flat tribometer measured an increase in wear life of chitosan/hydroxyapatite reinforced polyethylene over hydroxyapatite reinforced polyethylene and neat polyethylene. Do to the increased wear life, attributed to the improved adhesion at the filler-matrix interface, a biocomposite using 8% v_f hydroxyapatite and 2%v_f chitosan is considered a potential material for use in orthopedic implants.

Dedicated to my father.

Table of Contents

List of Figures

List of Tables

Acknowledgements

I would like to thank all those who helped me over the course of my work.

Professor Gary Halada and the Environmental Nanotechnology group for performing the Raman spectroscopy and the benefit of their experience with chitosan.

Professor Miriam Rafailovich, Vladamir Zaitsev and Seongchan Pack of the Polymers Engineering Laboratory for helping me with the compression molding and thermo gravimetric analysis.

Professor Sanjay Sampath and Brian Choi of the Center for Thermal Spray Research for their assistance with wear testing and the use of their tribometer.

James Quinn for his SEM images, which were invaluable to understanding my materials, and his insights into my work.

I would like to thank all my lab mates for their help and support with problems small and large. Specifically, I would like to thank Wei Zhao, for his help with AFAM testing, and Hani Mubarez, for his time spent compression molding samples to test.

Most of all, I would sincerely like to thank Professor Chad Korach for all his assistance with my thesis work. His patience, wisdom and guidance have been invaluable to me and I have learned a great deal under his mentorship. He is asset to any student and I cannot describe what a blessing it was to have him as my advisor.

Chapter 1
Introduction

Hydroxyapatite, polyethylene and chitosan are materials with proven applications in medical science and biomedical engineering. Hydroxyapatite is often used for its bioactive and bone like properties[1]. Chitosan is used for its biodegradable and antiseptic properties, often as a replacement for collagen[2]. Ultra high molecular weight polyethylene (UHMWPE) is used nearly universally in joint replacements due to its toughness, wear resistance and biocompatibility[3]. Using these materials together creates composites with advantageous properties, such as improved strength, toughness and bioactivity.

An osteoconductive bone paste of hydroxyapatite and chitosan has been designed for use in orthopedic and dental fillings[4]. Hydroxyapatite is used to create osteoblasts, the preferred method of promoting bone in growth. The chitosan matrix creates a scaffold which slowly dissolves in vivo. Also, chitosan's antiseptic properties help prevent infection at the implantation site. Compressive strength was shown to increase with an increase in hydroxyapatite content and a decrease in other fillers[4]. In other studies, flexural strength was shown to be highest with a chitosan content of 20% in a chitosan-calcium phosphate cement[5]. Other materials have been created with similar functions[6].

Composite hydroxyapatite/chitosan microspheres were created for use in the delivery of therapeutic agents in the human body[7]. These took advantage of the

osteoconductive nature of hydroxyapatite to target bones and similar areas, for direct delivery.

True tissue engineering has been investigated using a three dimensional biomimetic chitosan/glucose scaffold to seed hydroxyapatite.[8] This application is similar to the bone cement, except interest is taken in the optimal porosity of each phase and the matrix is designed to provide resources to promote growth.

Ultra high molecular weight polyethylene is the most common wear surface used in joint replacements due to its biocompatibility, toughness and low friction. Because of this widespread use, extensive research has been done on the tribology of UHMWPE. The wear behavior has been studied and it was concluded that while a pin on disk test shows the same mechanisms of wear as are found *in vivo*, the wear rate in a linear test is considerably lower than that in a multidirectional test due to wear hardening of the polyethylene[9]. Penetration of UHMWPE wear cups *in vivo* are a main cause of joint failure. While wear rates vary greatly, the average rate of penetration, the combination of wear and creep that causes the femoral head to actually penetrate the acetabular wear cup, was found to be 0.21 mm/year[10]. The other main form of implant failure is osteolysis, when bone degradation causes implant loosening. It has been shown that as wear particles released from the joint exceed 500 mm^3, problems with osteolysis occur[11].

Composites have been made of high density polyethylene (HDPE) to improve its strength and wear resistance. Investigation revealed that in addition to increasing the bulk modulus and strength, the inclusion of reinforcement reduced wear by improving the tribochemical behavior of polyethylene[12-14]. By increasing the adhesion of a transfer film to the wear counterface, reinforcing HDPE reduced adhesive wear. Bonfield *et al*[1,

15] introduced the hydroxyapatite reinforced HDPE composite as a bone replacement and did extensive work in optimizing its processing, strength and wear resistance. It was found that reinforcement of 10 vol.% provided the best improvement wear resistance. Ultimately, HDPE was found to have wear resistance too low to be a suitable material for hip replacements[16].

Attempts have been made to reinforce UHMWPE with hydroxyapatite. Compression molding a mixture of UHMWPE powder with similar sized hydroxyapatite particles yields improvements in strength and wear resistance with negligible effect on friction coefficient[17-18]. The main challenge with UHMWPE composites is mobilizing the long polymer chains which are extremely viscous, even above the melting temperature[19]. Because of this, poor there is poor interaction between the polyethylene and filler and interfacial strength is mainly due to mechanical interlocking.

A possible use for chitosan hydroxyapatite composites is as reinforcement for engineered UHMWPE composites. If hydroxyapatite reinforcement could be coated with chitosan, it could serve as a functional interface between HA and UHMWPE and improve strength and wear characteristics. This would have the advantage of using only biocompatible materials, which techniques such as swelling[20] and plasticizing lack.

The structural integrity of these composites is important. The purpose of this study is to investigate bonding between hydroxyapatite and chitosan and create biocomposites appropriate for use in load bearing applications. The materials are investigated for mechanical, function and chemical properties.

1.1 Materials

All materials were purchased from Sigma Aldrich. Materials were chosen for their mechanical and biocompatible properties. The goal is to create biocomposites which won't cause irritation in vivo, while maintaining the desired mechanical properties.

Hydroxyapatite is used for the main reinforcement in all composites. Hydroxyapatite ($Ca_5HO_{13}\ P_3$) is biocompatible and osteoconductive, meaning it will be actively absorbed into living bone tissue. It is a rigid material, with an elastic modulus (117 GPa) of over four times that of cortical bone (17-27 GPa). Hydroxyapatite particles are spherical in shape and on the order of 20μm in diameter. Each particle is comprised of a series of shells, as seen in Figure 1.1. Hydroxyapatite has a molecular weight of 205.31 AMU and a melting point of 1670 °C.

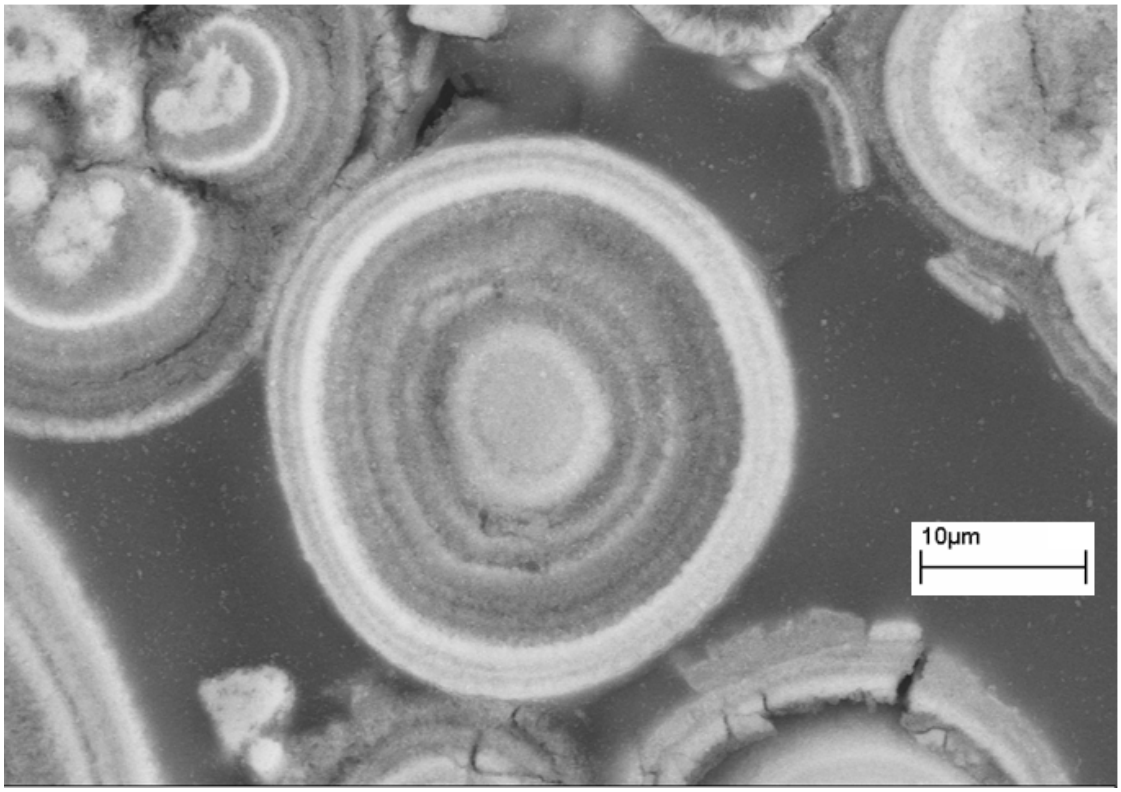

Figure 1.1: Polished cross section of hydroxyapatite particles embedded in epoxy.

To serve as the matrix in the biocomposite and act as an interlayer in polymer composites, chitosan ($C_{12}H_{24}N_2O_9$), an organic polymer, is used. It is produced from deacetylated chitin found in crab shells. Deacetylization shifts functionality from the acetyl groups to the amine groups. Chitosan is a biocompatible material due to its biodegradability and low toxicity. The chitosan used to manufacture composites in this study comes in a flake-like form with particles approximately 200 -1000 µm in size.

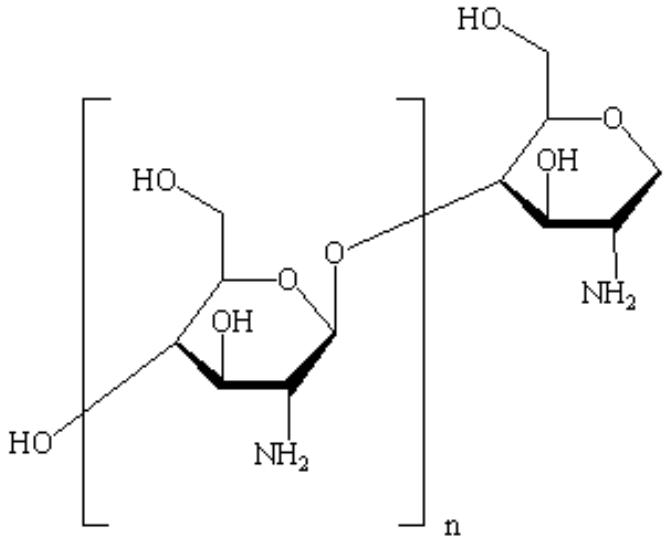

Figure 1.2: Diagram of the chitosan monomer.

To dissolve the chitosan, which comes in a solid form, the organic malic acid ($C_4H_6O_5$) is used. It has a molecular weight of 134.09 AMU and a melting point of 131°C. Malic acid is chosen for its biocompatibility and low toxicity and has successfully been used to dissolve chitosan in solutions.

Polyethylene ($[C_2H_4]_n$) is the main wear component in the biocomposites. The UHMWPE used comes as amorphous, spherical particles approximately sized 100 µm. It

has a density of 0.94 g/ml and a melting point of 146°C. It is a strong, tough material with an elastic modulus (E) of 1-2 GPa.

Table 1.1: Summary of material properties provided by the supplier[29-32].

	Chemical Formula	Molecular Weight (AMU)	Melting Point (°C)	Notes
Hydroxyapatite	$Ca_5HO_{13}P_3$	502.31	1670	Water Insoluble
Chitosan	$C_{12}H_{24}N_2O_9$	-	-	Deacetylated chitin
Malic Acid	$C_4H_6O_5$	134.09	< 150	
UHMW Polyethylene	C_2H_4	-	146	

Chapter 2
Chitosan-Hydroxyapatite Biocomposites

2.1 Processing and Fabrication of Chitosan-Hydroxyapatite Biocomposites

A chitosan-hydroxyapatite paste was fabricated by modifying the procedure developed by *Ito*[4]. The goal of modification of the previous work was to maximize the amount of hydroxyapatite reinforcement and minimize malic acid. Varying ratios of hydroxyapatite, chitosan and malic acid were used to create a range of composite pastes. Hydroxyapatite content was maximized because it is the main load bearing phase and has advantageous bioactive properties. Malic acid content was minimized because its main function is to dissolve chitosan and for the potential of irritation from low pH materials. Both chitosan/malic acid gels and chitosan/hydroxyapatite pastes were evaluated on processing ease and material homogeneity while trying to maximize hydroxyapatite % and minimize malic acid %.

Chitosan gels are made by dissolving chitosan flakes in a low concentration malic acid. Malic acid is dissolved in water by varying concentrations as seen in Table 1. Chitosan is mixed into the acid in a glass beaker with a spatula to create a gel. These concentrations were chosen by using the one to one gel created in *Ito* as the upper limit and lowering malic acid content to observe the limit of chitosan dissolution. The gel is allowed to rest at room temperature and laboratory air for 24 hours to allow the chitosan

to fully dissolve and the gel to thicken. After 24 hours the material is a thick, slightly yellow, and translucent gel. Water loss due to evaporation is shown in Table 1.

Table 2.1: Composition of chitosan gels with varying concentrations of malic acid and water loss due to evaporation of those gels. Gels 1 and 2 easily dissolved chitosan. Gel 3 failed to fully dissolve chitosan after 24 hours.

Gel	Water(g)	Malic Acid (g)	Chitosan (g)	Evaporated H_2O (g)	Final Weight
1	23.7	0.749	0.748	6.612	18.585
2	23.7	0.567	0.75	6.299	18.718
3	23.6	0.326	0.75	6.157	18.519

As received hydroxyapatite particles were added to the chitosan gel to create a composite paste. For each of the three chitosan gels, three different weights of hydroxyapatite were added to create nine unique composite pastes (Table 2). The hydroxyapatite particles are mixed with a spatula into the chitosan gel for 3 minutes. Care is taken to insure a good particle distribution throughout the paste. Once the hydroxyapatite is well distributed through the chitosan gel, the material was set aside to dry at room temperature in laboratory air. The paste fully dried in 3 days to form a bone like composite.

In addition to the nine composites described above, two separate composites were created for characterization experiments. Gel 2 was diluted with an additional 46.3 grams of water to create a thin film appropriate for AFAM testing. This was spread across a glass slide and approximately 5 mg of hydroxyapatite particles were mixed in to create individual particles coated with a chitosan film. Composite paste 2.2 was modified by using the same weight percentage of smaller, ~200 nanometer sized reinforcement

instead of the standard hydroxyapatite particles. This material was used for comparison in thermo gravimetric analysis (TGA).

Table 2.2: Components of pastes

Variation	1	2	3
Gel 1(g)	2.066	1.644	1.222
Ha(g)	1	1	1
Gel 2(g)	1.988	1.645	1.205
Ha(g)	1	1.005	1
Gel 3(g)	2.067	1.6	1.211
Ha(g)	1	1	1

Table 2.3: Components by mass of 9 unique pastes after drying

Paste	Malic Acid	Chitosan	Hydroxyapatite
1.1	7.14%	7.13%	85.73%
1.2	5.85%	5.84%	88.31%
1.3	4.48%	4.48%	91.04%
2.1	5.28%	6.99%	87.73%
2.2	4.45%	5.88%	89.67%
2.3	3.36%	4.45%	92.18%
3.1	3.25%	7.47%	89.28%
3.2	2.58%	5.93%	91.49%
3.3	1.99%	4.58%	93.43%

2.2 Characterization

Malic acid and chitosan were added to hydroxyapatite in varying amounts, as previously described, to determine two primary processing effects: First, how malic acid concentration affects the dissolution of chitosan and the formation of a chitosan gel. Second, to determine at what hydroxyapatite concentration the particles begins to dominate the composites.

Three different concentrations of malic acid were dissolved in chitosan to fabricate chitosan gels. The 1:1 and 0.57:0.75 concentrations of malic acid to chitosan formed thick and homogenous chitosan gels. The 0.33:0.75 concentration malic acid:chitosan was thinner and a small amounts of chitosan appeared to remain undissolved in the final gel. Comparison of the three concentrations shows that the minimum malic acid concentration necessary to fully dissolve the chitosan is greater than a 1:2 ratio.

The chitosan gel was mixed with the hydroxyapatite particles at concentrations varying from 2:1 to 1.2:1 chitosan:hydroxyapatite to form pastes. During kneading, the gels exhibited varying levels of homogeneity. Samples fabricated from the two gels of higher malic acid concentration mixed well with 2:1 and 1.6:1 ratios of chitosan:hydroxyapatite, but not 1.2:1 ratios, at which point the paste became significantly thicker and harder to achieve homogeneity. The gel with lowest concentration of malic acid mixed poorly with the hydroxyapatite with small lumps forming in the mixture implying poor distribution of hydroxyapatite throughout the paste.

The limit for optimum hydroxyapatite mixture appears to be made with a mixture of Gel 2 to hydroxyapatite in ratio of 1.6:1, made in sample 2.2. The goal of this work is

to maximize the amount of rigid hydroxyapatite reinforcement and minimize the amount of non-structural malic acid. For the remainder of this work, the fabricated biocomposites will follow a composition of 4.45% malic acid, 5.88% chitosan and 89.67% hydroxyapatite because this is the limit of chitosan dissolution and hydroxyapatite particle distribution homogeneity.

2.3 SEM of Chitosan/Hydroxyapatite Composites

SEM micrographs were taken to examine the chitosan/hydroxyapatite composite preparation. Samples were fractured to study the chitosan-hydroxyapatite adhesion. Both sample surfaces and fracture surfaces were examined by SEM to investigate surface morphology, particle distribution, film thickness and distribution and failure modes. Materials were prepared for SEM by mounting samples on a layer of carbon tape and coating them with a layer of gold to enhance electron conductivity.

2.3.1 SEM Surface Images

The surface of neat hydroxyapatite and chitosan/hydroxyapatite composite samples are depicted in Figures 2.1-2.6. Figures 2.2, 2.3, and 2.4 are the surface of sample 1.1 (7% malic acid, 7% chitosan, 86% hydroxyapatite). In comparison with the uncoated hydroxyapatite in Figures 2.1 and 2.2, a distinct coating has covered the hydroxyapatite particles. Two points illustrate this: First, the surface texture of the particles changes from discrete and smooth to dull and lumpy. Second, a film can be seen stretching between particles, as in Figures 2.4 and 2.5.

Comparing the micrographs of sample 1.1 with sample 3.3(2% malic acid, 5% chitosan, 93% hydroxyapatite) illustrates how different ratios of chitosan, malic acid and

hydroxyapatite affect the morphology of chitosan/hydroxyapatite composites. Sample 1.1 (Figures 2.2 and 3) is shown to have a much thicker chitosan coating than sample 3.3 (Figures 2.5 and 2.6) which is due to the increased concentration of both malic acid and chitosan. Higher chitosan concentration offers more material to coat the particles and higher malic acid concentration better dissolves and distributes the chitosan for a better quality coating. Sample 3.3 still has a good distribution of chitosan within the hydroxyapatite particles and displays the stretching film and change in surface texture to show the chitosan is coating the particles.

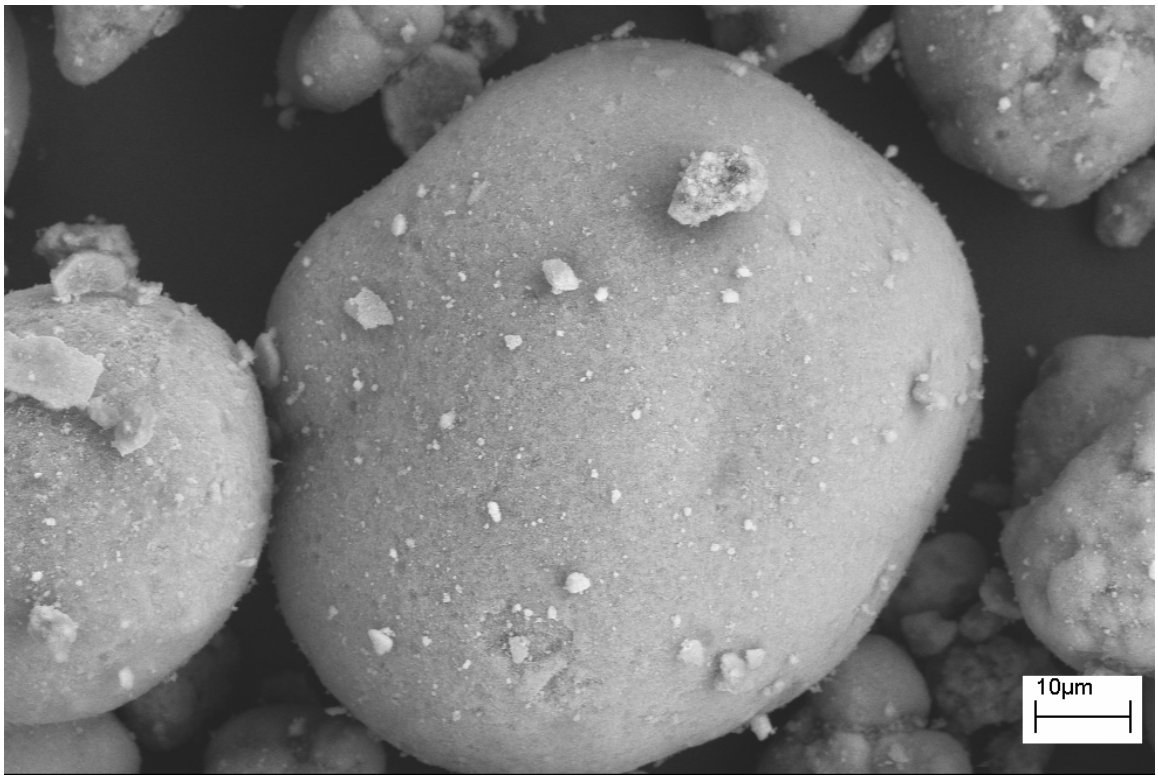

Figure 2.1: Uncoated hydroxyapatite particles on carbon tape substrate.

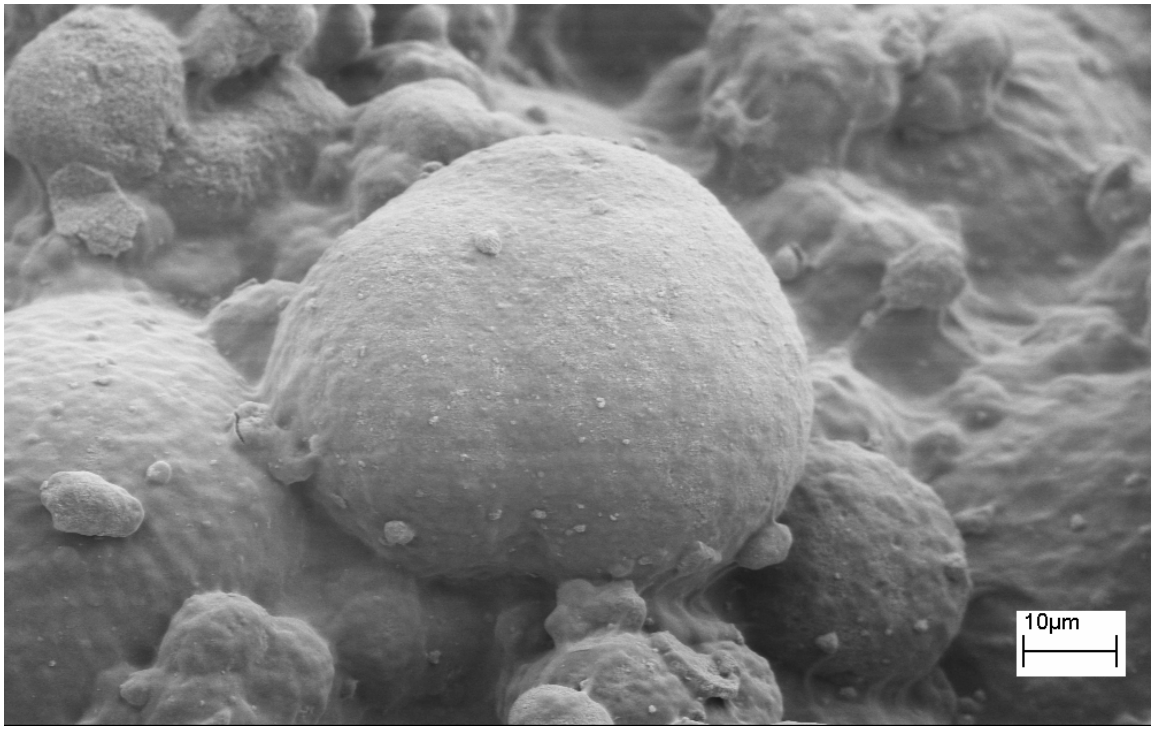

Figure 2.2: SEM micrograph of chitosan/hydroxyapatite composite sample 1.1. The surface texture has become duller in comparison with Figure 2.1, indicating the presence of a chitosan coating.

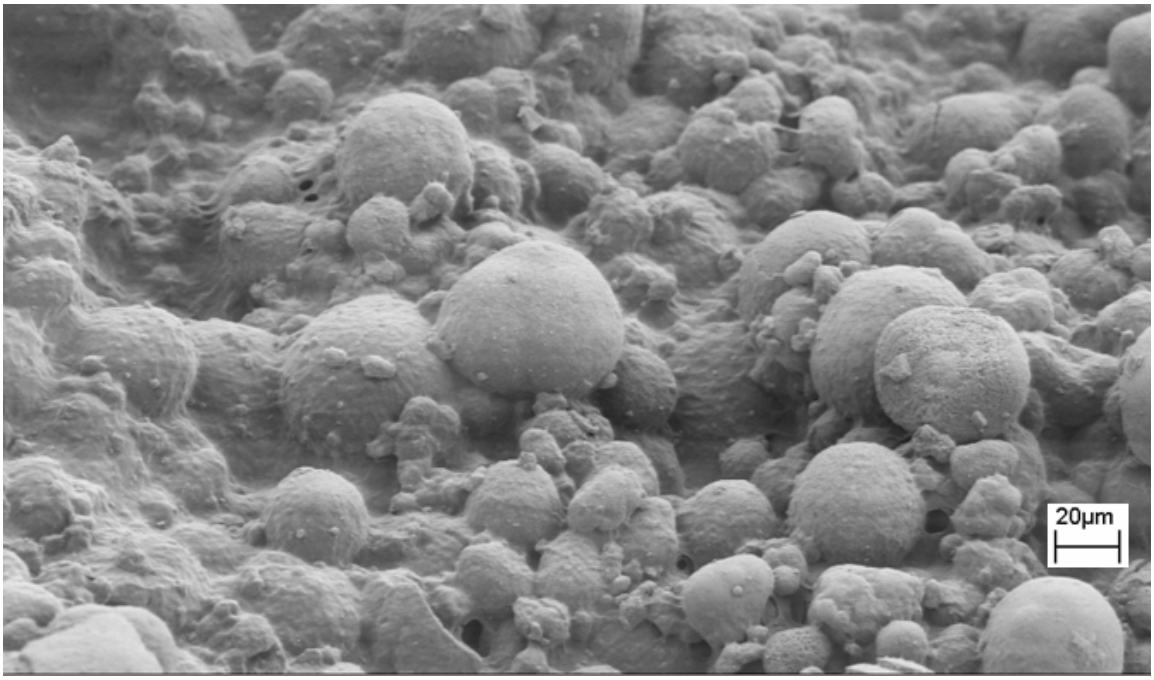

Figure 2.3: SEM micrograph of chitosan/hydroxyapatite composite sample 1.1. The thick, even coating of chitosan can be seen on and between the hydroxyapatite particles.

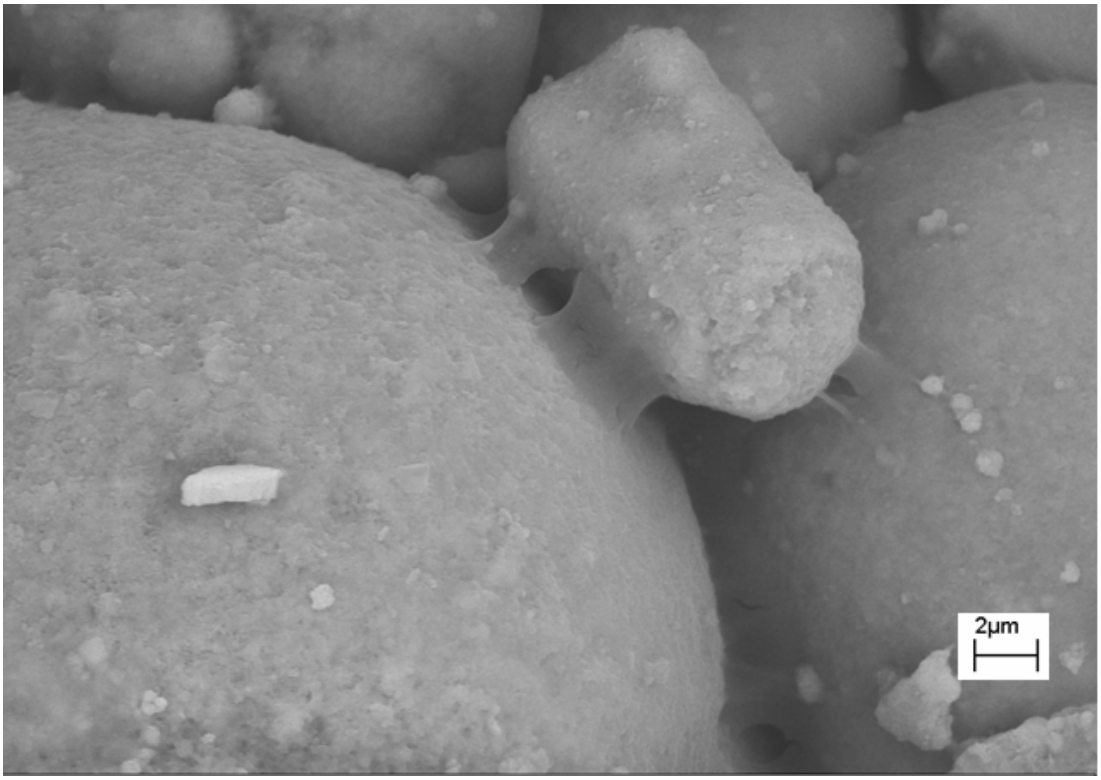

Figure 2.4: SEM micrograph of chitosan/hydroxyapatite composite sample 1.1. Chitosan film can be seen stretched between hydroxyapatite particles.

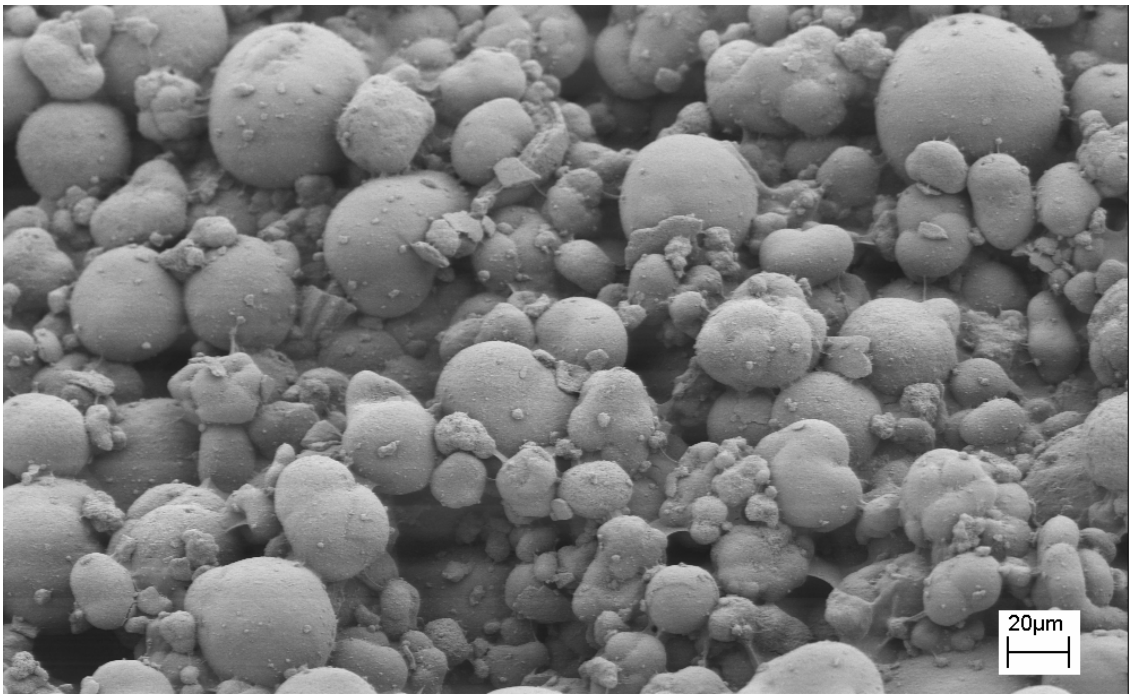

Figure 2.5: SEM micrograph of chitosan/hydroxyapatite composite sample 3.3. Less chitosan coats the surface of the composite and bare particles of hydroxyapatite can be seen.

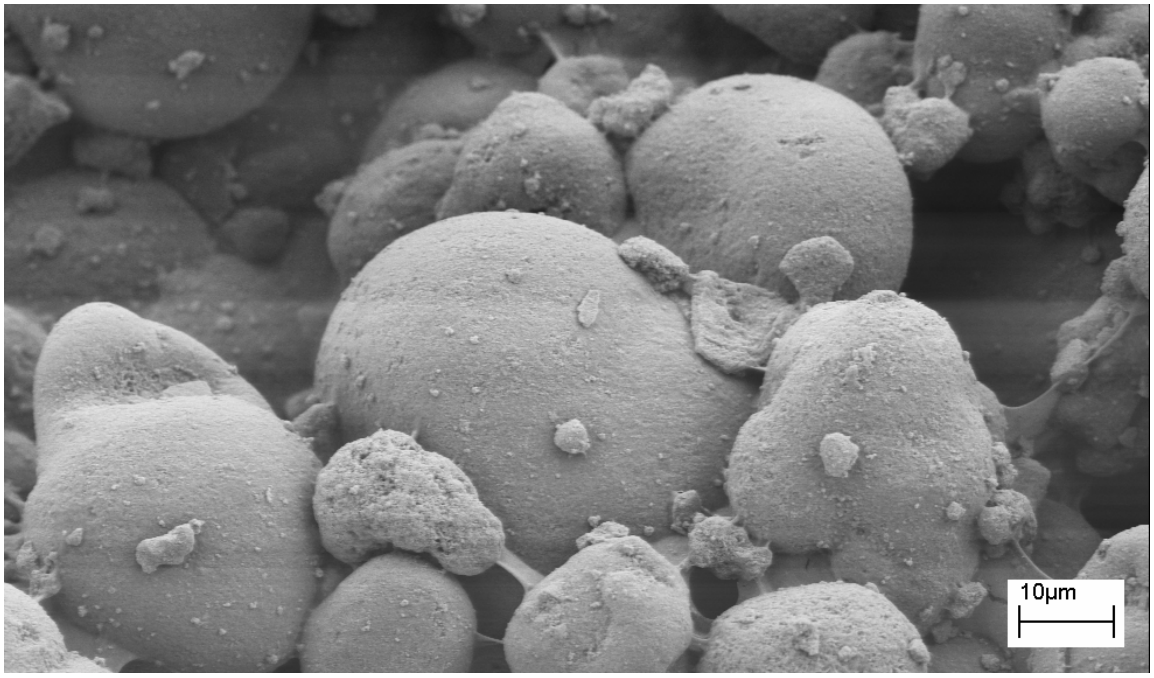

Figure 2.6: SEM micrograph of chitosan/hydroxyapatite composite sample 3.3.

2.3.2 SEM Fracture Surface Images

Images of chitosan/hydroxyapatite fracture surfaces can be seen in Figures 2.7-2.10. Fracture surfaces were obtained from a simple two point bending of the composites. The composites were brittle and fractured easily. Composite thickness and length were kept consistent to insure a similar bending moment and stress on the sample cross sections.

Sample 2.2 (4% malic acid, 6% chitosan, 90% chitosan) was examined, with Figure 2.7 showing the fractured sample cross section. It is clear from the micrograph that the sample has voids and high porosity between the particles of hydroxyapatite. Also, there are many hydroxyapatite particles which have undergone internal cohesive failure and there is little evidence of particle pull-out or adhesive failure at the chitosan-hydroxyapatite interface. Figure 2.8 is broken shells of hydroxyapatite coated with a thick layer of chitosan. The chitosan well coats the hydroxyapatite and fills the space

between the particles. As is seen from Figure 2.8, the chitosan-hydroxyapatite bond strength is evident with the hydroxyapatite particle cohesively failing and the chitosan-hydroxyapatite bond remaining well intact.

Figure 2.9 is a particle of hydroxyapatite on the interior of the composite. The particle is not coated with a thick coating of hydroxyapatite, but instead a thin film. This film is on the order of 300nm thickness, highlighting how well the chitosan coats the hydroxyapatite. Even when a large amount of chitosan is not present, the particles still have a thin coating, which serves as a binding matrix between the particles.

Figure 2.10 is a particle of hydroxyapatite coated with chitosan which has been broken in two. The chitosan well coats the hydroxyapatite, despite the obvious force necessary to crack the hydroxyapatite shell. The chitosan has begun to peel away from the hydroxyapatite, but only in a region where the hydroxyapatite shell is already cracked and is likely due to the high stress concentration at the interface. This demonstrates that the force (and thus stress) necessary to delaminate the chitosan from the hydroxyapatite is greater in magnitude that the cohesive strength of the chitosan film and the hydroxyapatite particles.

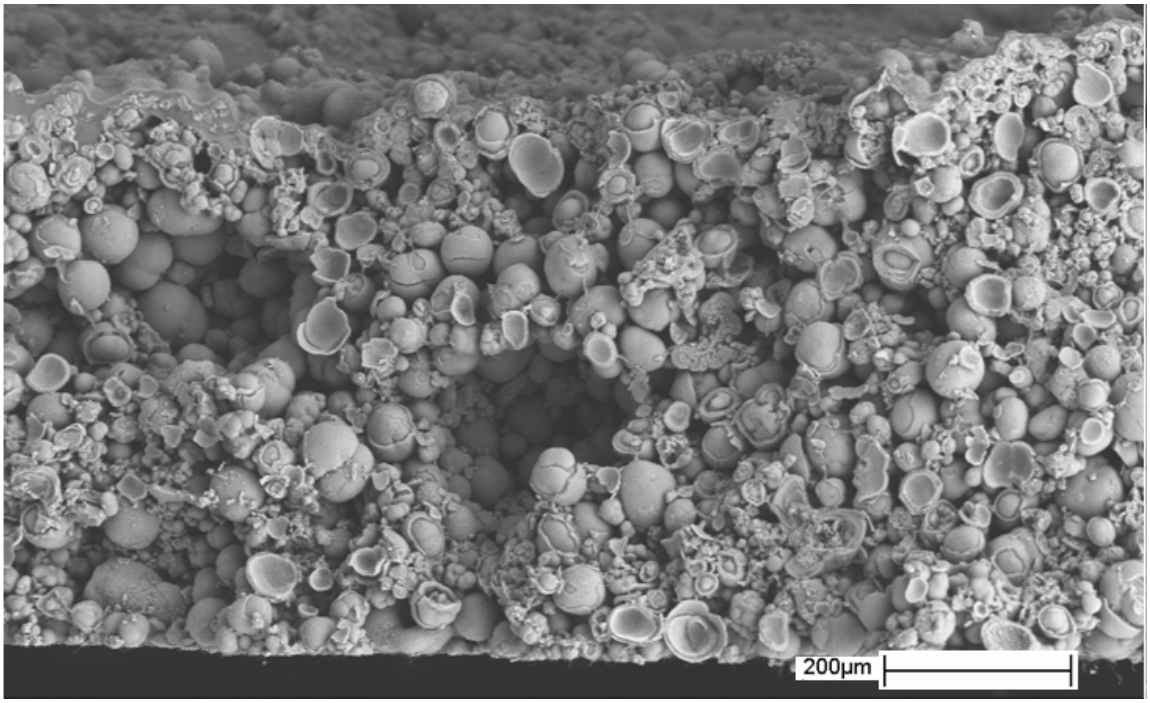

Figure 2.7: SEM image of Sample 2.2 fracture surface. The composite has large voids and high porosity.

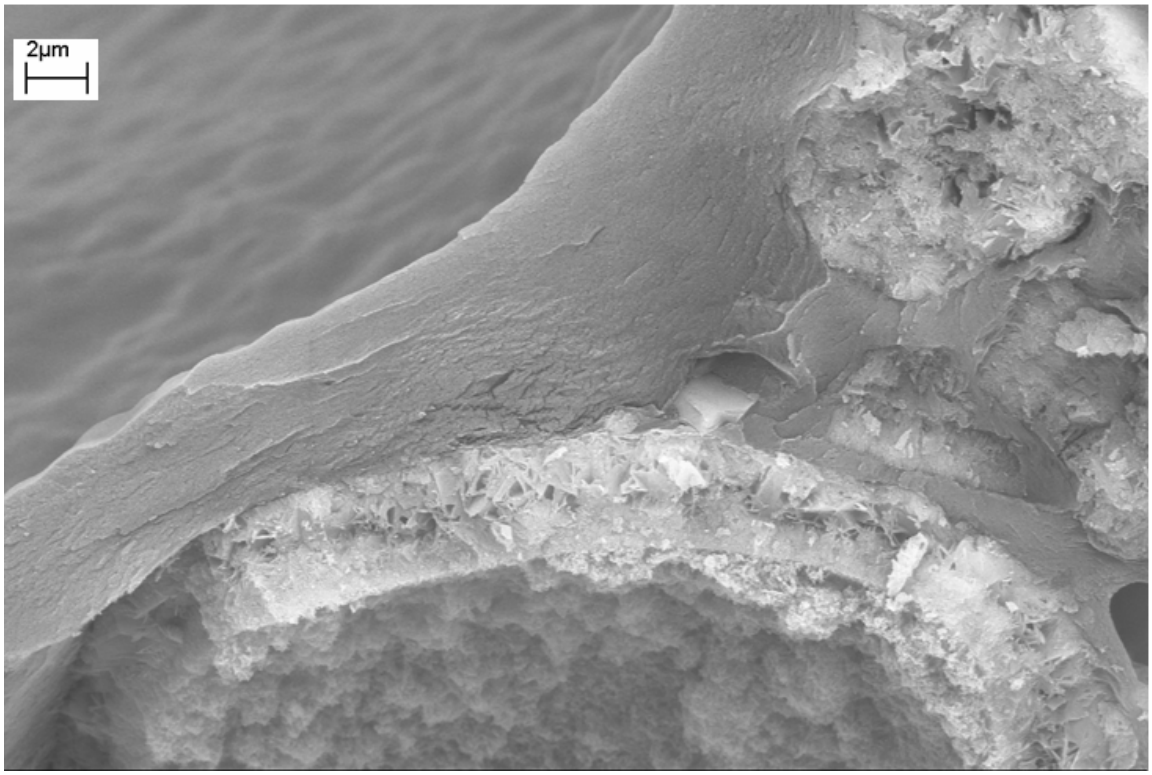

Figure 2.8: SEM image of Sample 2.2 fracture surface. The chitosan coating is well adheared to the hydroxyapatite shell.

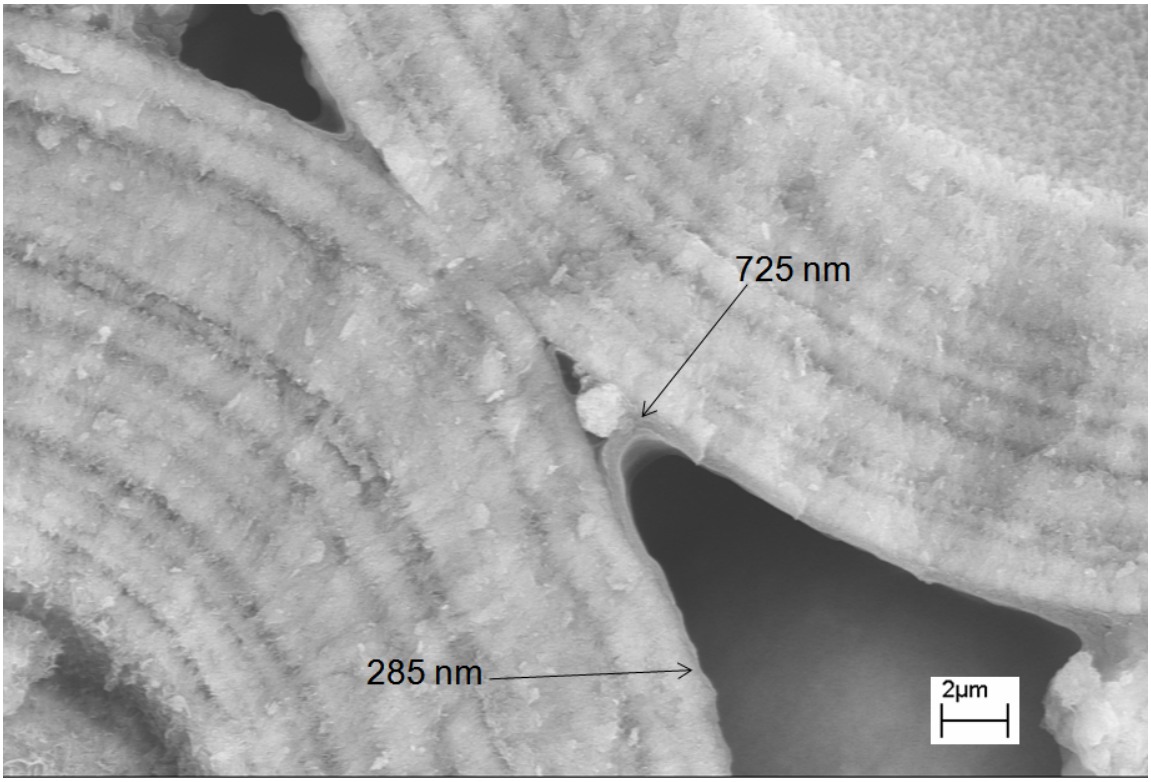

Figure 2.9: SEM image of Sample 2.2 fracture surface, showing film thickness.

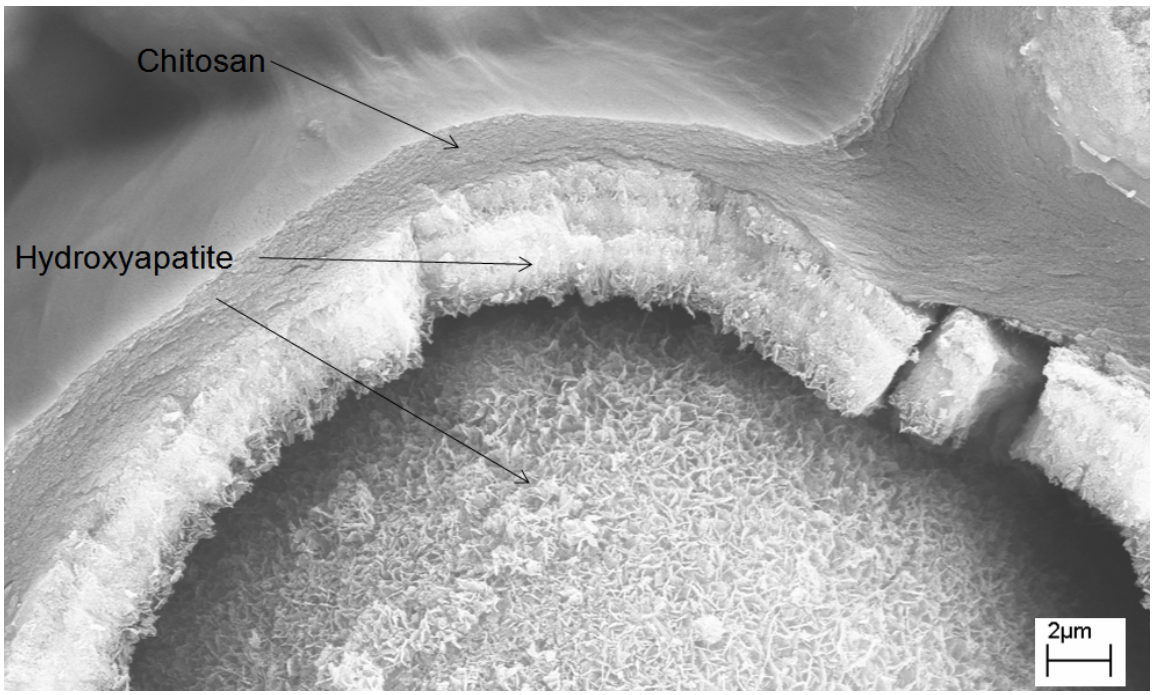

Figure 2.10: SEM image of Sample 2.2 fracture surface. A section of the hydroxyapatite shell has fracture before the particle could delaminate from the chitosan coating.

2.4 Raman Spectroscopy of Chitosan/Hydroxyapatite Composites

Raman spectroscopy was performed to investigate the chemical bonding in the chitosan-hydroxyapatite composites. Raman spectroscopy uses a laser to excite the atomic bonds in a material. A detector collects the reflected light and a comparison between the collected and original wavelengths gives information about the phonon modes in the system.

A Thermo Nicolet Almega spectrometer was used with a 532nm wavelength laser at 30 mW. 128 scans were taken over a 3600 Raman shift. Four samples were tested, one of neat hydroxyapatite particles and three chitosan/hydroxyapatite composites with three chitosan:hydroxyapatite ratios increasing hydroxyapatite content.

The Raman spectra for the three chitosan/hydroxyapatite composites is shown in Figure 2.11. The spectra show four distinct peaks corresponding to four phosphate vibrational states. These four peaks demonstrate that the hydroxyapatite is Raman active. The overall rise in Raman intensity is due to the chitosan fluorescence which increases with chitosan concentration.

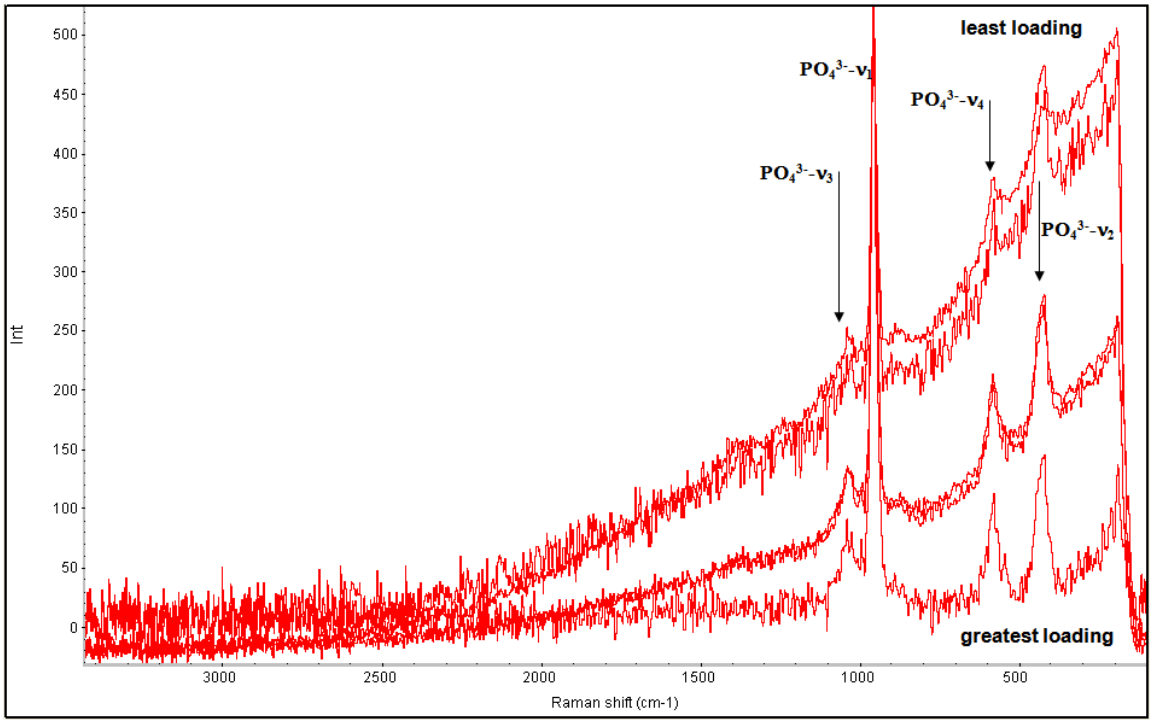

Figure 2.11: Raman spectra from chitosan/hydroxyapatite composites of various hydroxyapatite loadings

Raman spectra comparing the neat hydroxyapatite particles to the chitosan/hydroxyapatite composites can be seen in Figure 2.12. A small but repeatable shift in the $PO_4^{3-}\nu_1$ Raman peak is present, due to interaction between the phosphate groups in hydroxyapatite and the amine groups in the chitosan/malic acid coatings. This peak shift indicates that there is good chemical surface interaction between the hydroxyapatite and chitosan in the composites and that the binding is more than a weak interaction. This provides an understanding of why the chitosan and hydroxyapatite fail cohesively before the chitosan delaminates from the hydroxyapatite particle surface, previously shown in the composite fracture surface images.

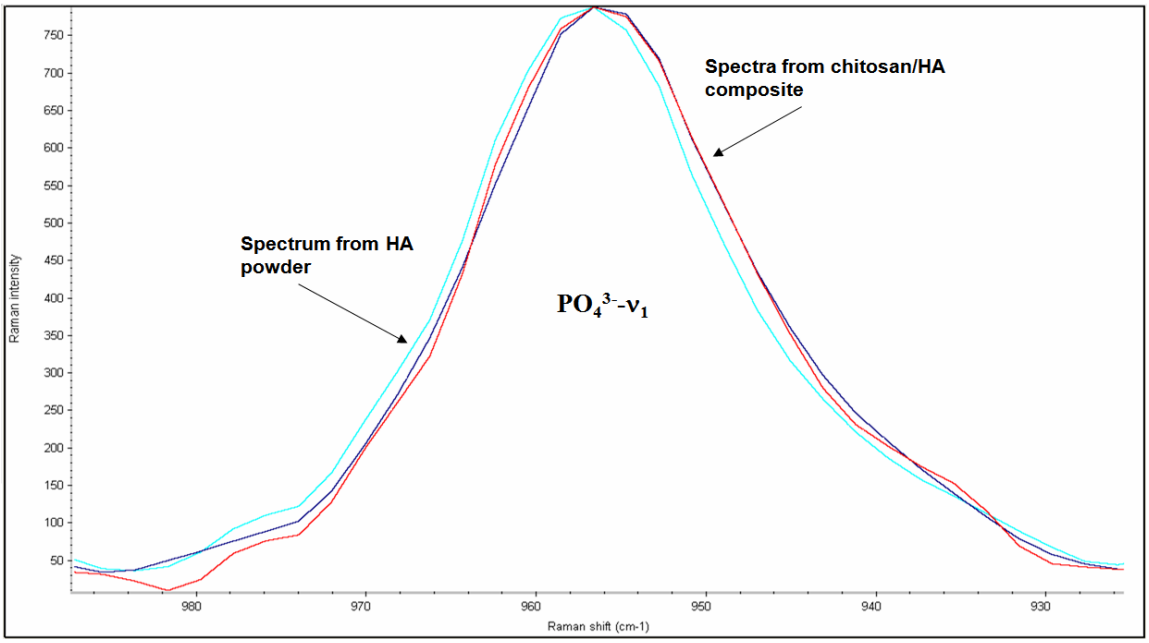

Figure 2.12: Raman spectra comparing hydroxyapatite powder and hydroxyapatite/chitosan composites

2.5 Thermo Gravimetric Analysis

Thermo Gravimetric Analysis (TGA) is used to characterize the thermal degradation of the composites. In addition to giving information about a material's melting and degradation points, TGA can be used to indicate a shift in overall material composition when used in comparing materials.

A Mettler Toledo TGA/SDTA 851 was used for these procedures. A small sample of less than 25mg was heated in a furnace while sample mass was measured with an analytic scale. The furnace was purged with nitrogen gas and heated to 850 °C temperature, well above the expected point of thermal degradation of both chitosan and malic acid. During heating, sample mass was recorded at 50 second intervals. The results reveal the thermal degradation curve associated with that material.

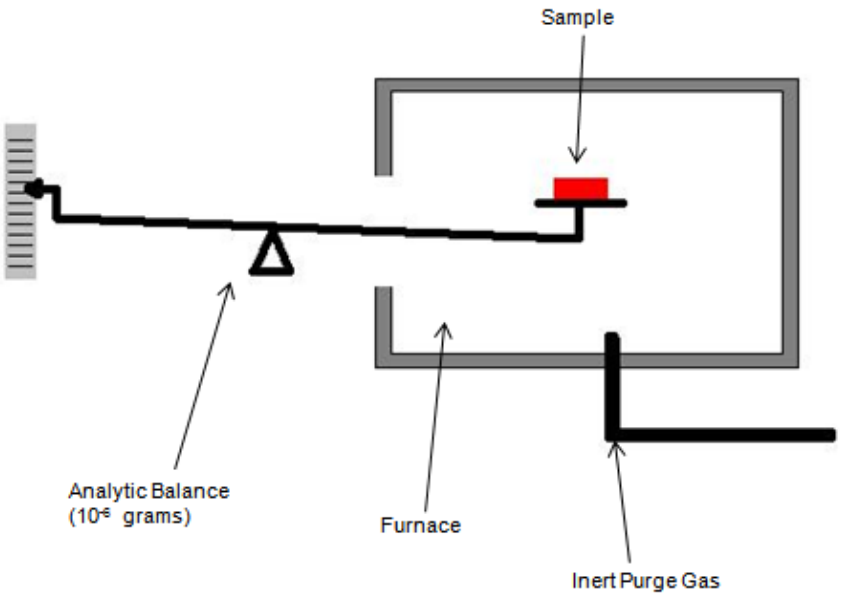

Figure 2.13: TGA testing system schematic.

TGA was performed on three samples: a neat chitosan gel, a composite with 20 μm-diameter hydroxyapatite reinforcement and a composite with 200 nm-diameter

hydroxyapatite reinforcement, with material composition seen in table 2.4. Two different types of hydroxyapatite were used to investigate if a difference in surface area would affect material properties. A shift in particle radius of 10^2 times corresponds to a shift in surface area (and thus surface interactions) of 10^4, a large enough increase that any potential changes could be evident.

Table 2.4: Composite composition for TGA analysis.

	Chitosan	Malic Acid	Ha
Neat Gel	57.03%	42.97%	0.00%
200nm Ha/Gel	8.43%	6.37%	85.19%
20µm Ha/Gel	8.41%	6.36%	85.23%

The temperature-mass curves for three different samples can be seen in Figures 2.14 and 14. The graph depicting the absolute change in mass has been shifted to depict the percent change in mass per unit mass lost. This graph illustrates an important observable detail. The degradation behavior changes drastically between the neat chitosan gel and the composites. The neat chitosan is more resistant initially to heat, but then degrades precipitously at about 200 °C. The composites are more resistant to thermal degradation, indicating that chitosan has bonded with hydroxyapatite. This shift in thermal degradation indicates that the chitosan-hydroxyapatite composites are not formed simply by a mechanical interface between the two phases, but by bonding between the two materials.

No significant shift in thermal degradation occurred with a change in hydroxyapatite surface area. Figure 2.15 shows a slight deviation between the two different hydroxyapatite reinforcements. This could be due to poor mixing of the

chitosan gel and 200nm hydroxyapatite, leading to large inclusions of chitosan and malic acid.

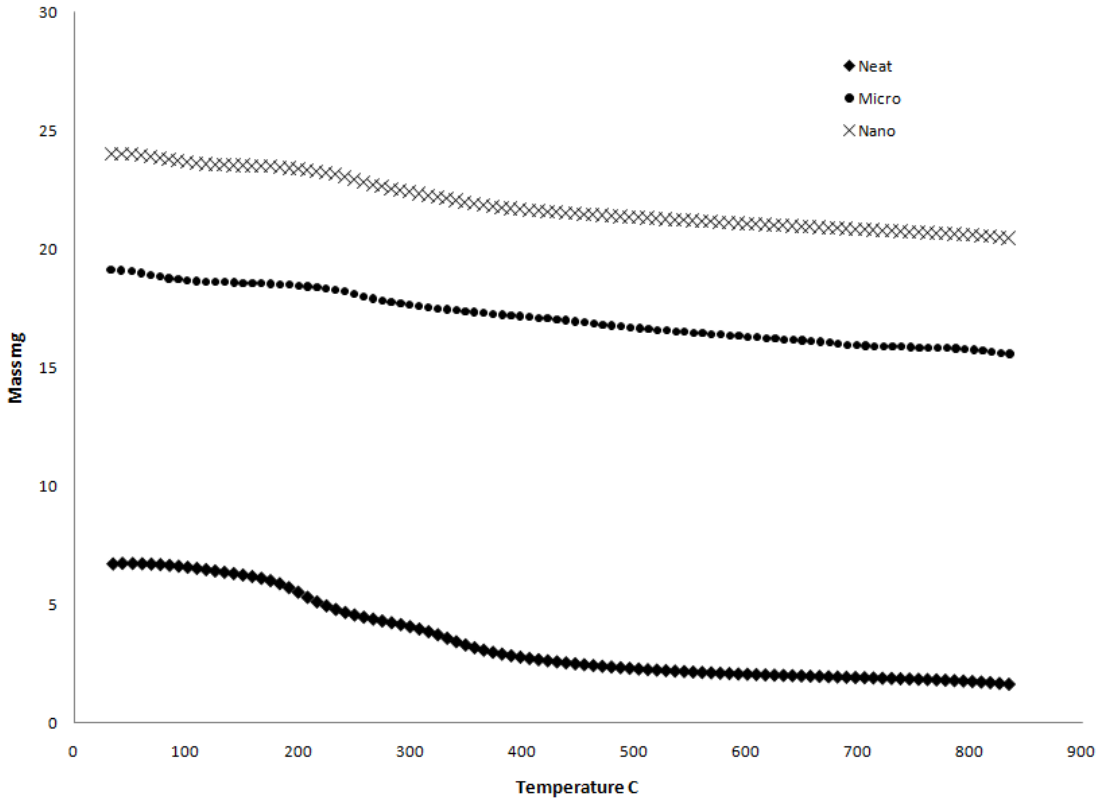

Figure 2.14: Thermal degradation curve of a neat chitosan film, chitosan reinforced with 20µm hydroxyapatite particles, and chitosan reinforced with 200nm hydroxyapatite particles. The mass lost from both composite samples corresponds with the amount of chitosan-malic acid gel originally added to the materials.

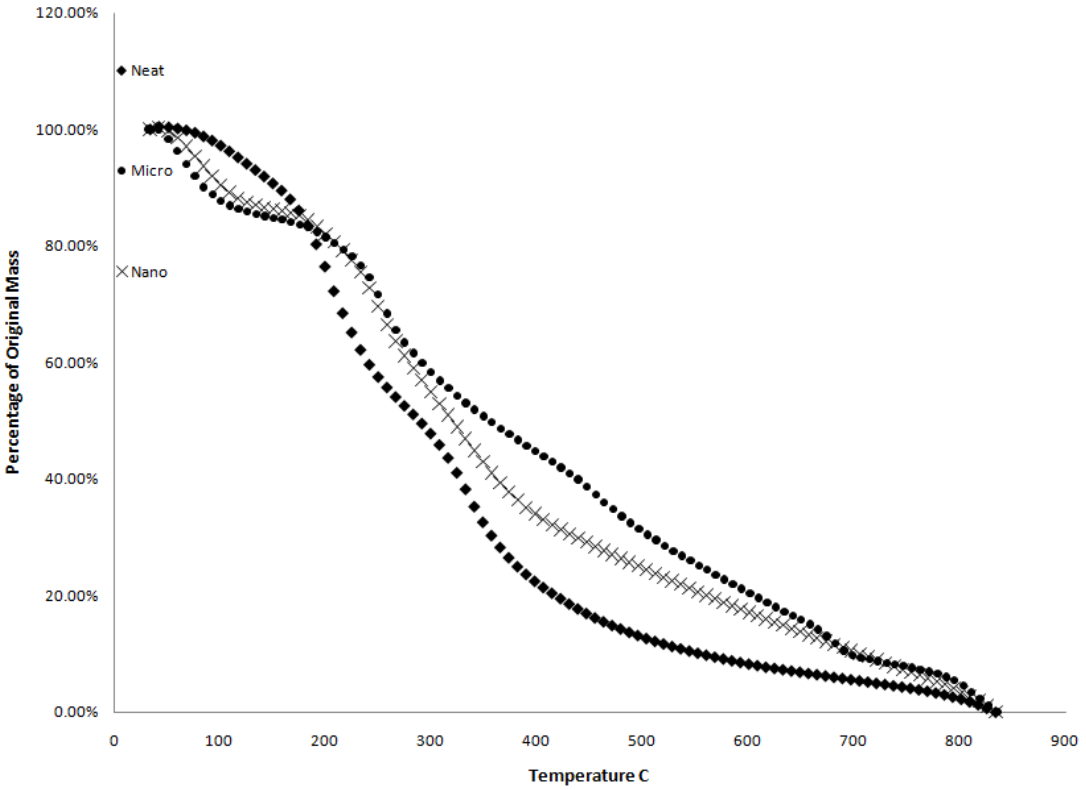

Figure 2.15: Thermal degradation curve of a neat chitosan film, chitosan reinforced with 20µm hydroxyapatite particles, and chitosan reinforced with 200nm hydroxyapatite particles, shifted to represent the percent change in mass per unit mass lost. Composites show a shift in behavior, initially more susceptible to thermal degradation than chitosan, then more resistant at higher temperatures.

2.6 AFAM of Chitosan/Hydroxyapatite Composite Films

To investigate the mechanical response of each phase in the chitosan-hydroxyapatite composites, atomic force acoustic microscopy (AFAM), is used to characterize the materials. AFAM utilizes ultrasonic frequency oscillations to excite a sample while in contact with an atomic force microscope cantilever tip (Figure 2.13) and has been used to study different phases in fiber reinforced composites[21].

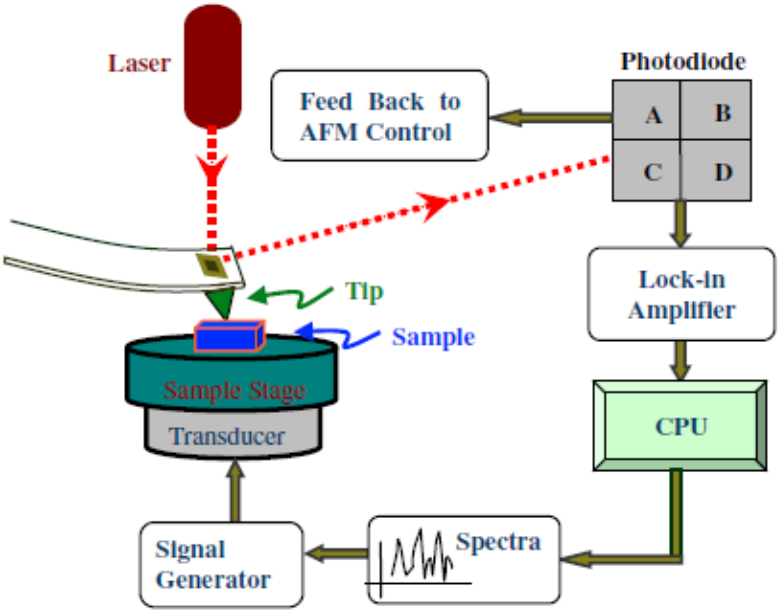

Figure 2.16: Schematic of AFAM setup showing location of sample on ultrasonic transducer.

Three samples were tested: a chitosan film, hydroxyapatite particles, and a thin film hydroxyapatite-chitosan composite. The thin film sample was prepared as described earlier in order to isolate individual particles of coated hydroxyapatite (Figure 2.14). The surface of an individual particle was scanned to isolate a flat surface at the particle apex for which to perform testing. Three hydroxyapatite particles were tested and two coated particles were tested, with three independent measurements performed on each particle.

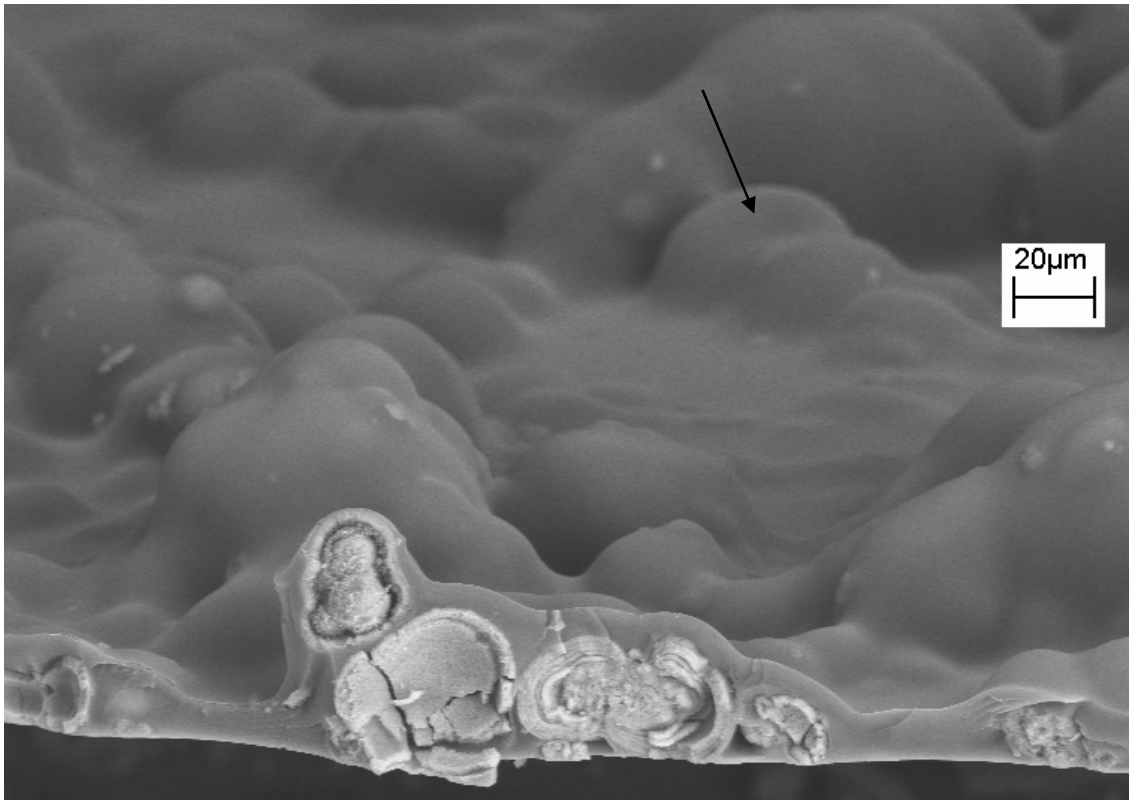

Figure 2.17: Image of thin film chitosan-hydroxyapatite composite for AFAM testing. Measurements were taken from the apex of individual coated hydroxyapatite particles. The arrow is indicating the type of feature that measurements were taken from.

AFAM is performed by insonifying a sample mounted on an ultrasonic transducer that emits longitudinal acoustic waves, in conjunction with an atomic force microscope (AFM) (NT-MDT SolverProM). To calculate the elastic mechanical response of the materials with AFAM, the tip-sample contact stiffness is determined by a vibrational model of the excited cantilever. The AFM cantilever is modeled as a clamped beam with a distributed mass that can vibrate in different modes, such as flexural, torsional, and extensional. Closed form solutions of the equations of motion have been used in flexural and torsional vibration modes for analysis of the free vibrations. If the beam is fixed at a length L_1 and coupled to a surface through a linear spring with stiffness k*, the equations of motion can be solved analytically using a simplified beam contact model as long as

amplitudes are sufficiently small. For larger amplitudes, a non-linear representation of the surface forces would be necessary. The contact stiffness, k*, represents the forces due to tip-sample contact. A representative characteristic equation for the modal flexural stiffness is given as:

$$\frac{k^*}{k_c}\left[\begin{array}{l}-(\cosh k_n L_1 \sin k_n L_1 - \sinh k_n L_1 \cos k_n L_1)(1+\cos k_n L' \cosh k_n L') \\ +(\cosh k_n L' \sin k_n L' - \sinh k_n L' \cos k_n L')(1-\cos k_n L \cosh k_n L)\end{array}\right] = 2\frac{(k_n L_1)^3}{3}(1+\cos k_n L \cosh k_n L) \quad (2.1)$$

where k* is the tip-sample contact stiffness, L is the total cantilever length, L1 is the tip position along the cantilever, and L' = L - L_1. The modal contact stiffness, k_n, is given by Eq. (2),

$$k_n = c_c\sqrt{f_n} \quad (2.2)$$

where

$$c_c = \sqrt{\frac{48\pi^2\rho}{b^2 E_i}} \quad (2.3)$$

and

$$k_c = \frac{E_i b^3 a}{4L_1^3} \quad (2.4)$$

and f_n are the vibrational frequencies for modes n = 1, 2, . . ., c_c is a characteristic cantilever constant, k_c is the cantilever spring constant, E_i (= 169 GPa) is the modulus of the cantilever material (silicon), ρ is the mass density of the cantilever material, and b is the cantilever height. Typical values of cantilever spring constants used in the AFAM measurements are larger than used for contact imaging, allowing higher normal loads to be applied to the contact interface while retaining small cantilever deflections. If smaller k_c values are used, the adhesive interaction forces between the AFM tip and the sample

surface are on the same order or larger than the contact forces applied by the cantilever. Viscous damping and lateral forces can be added into the theoretical model though their influence on k^* is small compared with the normal forces and errors generated by tip geometry and position. The resonance frequencies are sensitive to the applied normal loads and increase with applied load due to a stiffer contact created between the tip and sample, though are stable within a certain range of loads.

A Hertzian contact model provides the elastic modulus of the sample surface, after obtaining the contact stiffness. In the three dimensional Hertz analysis, the contact is assumed to be a parabolic indenter in contact with a flat surface. The indenter tip and the surface have elastic modulus of E_i and E_s, and Poisson's ratios of ν_i (= 0.33) and ν_s (= 0.36), where *i* and *s* represent the indenter and the surface, respectively. For a statically applied force, $F_c = k_c \, x \, \Delta z$, where Δz is the cantilever deflection. In our experiments the tip-sample forces F_c are sufficiently large to overcome surface interaction forces to ensure that the elastic contact forces are the main contribution to the analysis. For small deflections, the radius of contact, a_c, and the effective elastic modulus, E^*, are given as,

$$a_c = \sqrt[3]{\frac{3F_c R}{4E^*}} \qquad (2.5)$$

$$\frac{1}{E^*} = \frac{1-\nu_s^2}{E_s} + \frac{1-\nu_i^2}{E_i} \qquad (2.6)$$

where R is the radius of curvature of the indenter tip which is measured by SEM. Using Eq. (5) and the mutual approach between surfaces, $= \frac{a^2}{R^*}$, the contact stiffness can be

represented by

$$k^* = \sqrt[3]{6E^{*2}RF_c} \qquad (2.7)$$

and relates the contact stiffness to the sample surface elastic modulus (E_s) by Eq. (6), and is a function of the applied contact force and the radius of curvature of the indenter tip.

Atomic force acoustic microscopy (AFAM) was used to measure the nano-scale material elasticity (E) of three samples: a chitosan film, hydroxyapatite particles and chitosan coated hydroxyapatite particles. Elastic modulus for the three samples was calculated from the measured contact stiffness across the same modal frequency using Eq. (7).

Table 2.5: Material elasticity as measured by AFAM.

Material	Elastic Modulus (Gpa)	Frequency Shift (kHz)
Hydroxyapatite particles	70.1	1970
Chitosan Coated Hydroxyaptite	10.7	850
Chitosan Film	9.43	850

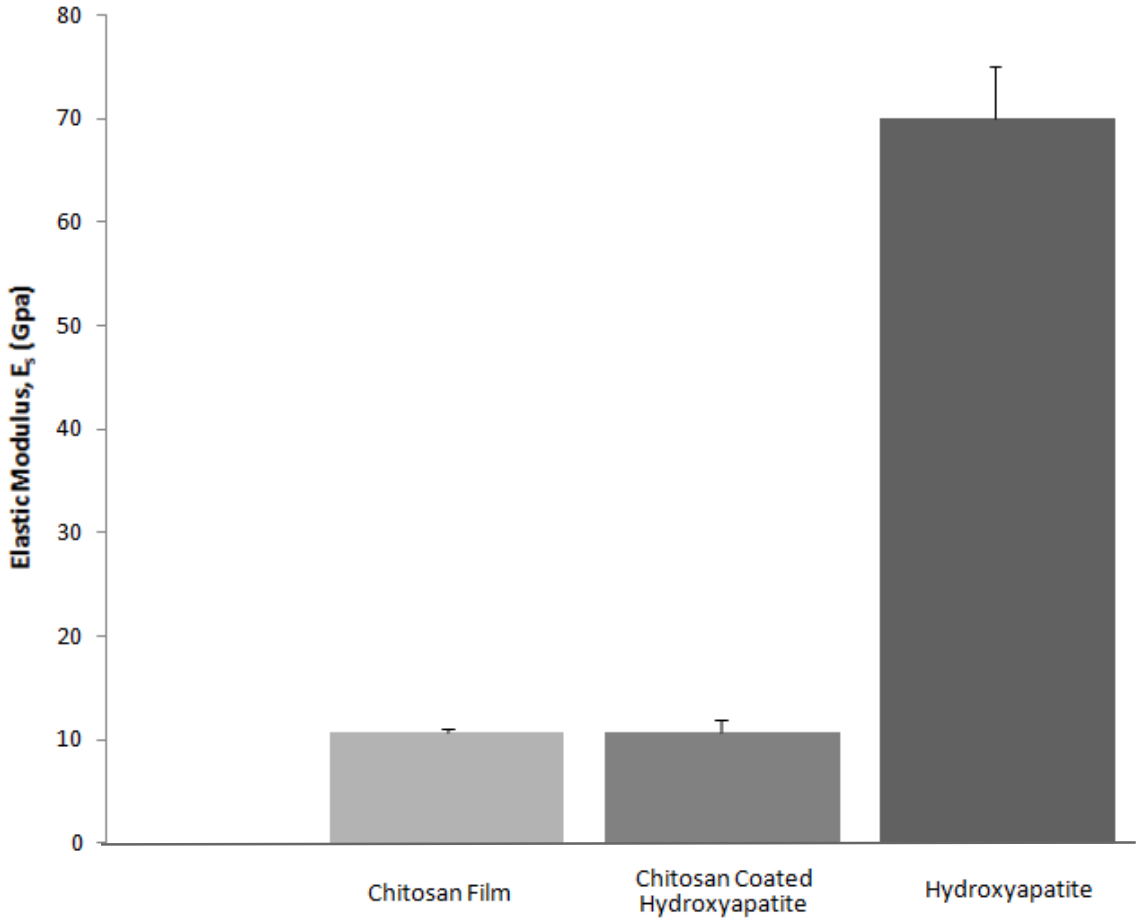

Figure 2.18: Material elasticity as measured by AFAM. The stiffness of both a chitosan film and chitosan coated hydroxyapatite particles is about on seventh that of uncoated hydroxyapatite.

The chitosan film is measured to have an elastic modulus significantly below that of hydroxyapatite. Whether bonded to hydroxyapatite or as a neat film, chitosan has a value of E_s of approximately 10 GPa or about one seventh the measured value of hydroxyapatite. Furthermore, in comparison with a known value of polyethylene stiffness of 1.7 GPa[22], the chitosan film is approximately 6 times stiffer. Since chitosan has a modulus intermediate of that of UHMWPE and hydroxyapatite, it could be used to create a functional layer between the two phases and increase the overall strength of a composite.

Chapter 3
Reinforced Polyethylene Composites for Wear Applications

3.1 Procedure for Making Thermoplastic Polyethylene Composites

Polyethylene composites were formed using solid state mixing and compression molding. Composites were made of various volume fractions to investigate how reinforcement loading affects wear resistance. It has been previously show that there is a limit near 15% v_f hydroxyapatite for optimal wear resistance[16, 18], so composites were made below this amount.

Composites are defined by their volume fraction, but components were measured by mass, as porosity may change during compression molding. A working volume of the mold is determined, the volume fraction of components selected and the necessary mass of each component determined by its density. In this study, the following component masses were used for a 2”x4”x0.25” mold:

Table 3.1: Dry components used in composites

	PE (g)	Ha (g)	Ha/Chitosan composite (g)
PE	40	0	0
10% Ha	25.38	9.413	
15% Ha	33.93	5.966	
5% Ha composite	33.93		5.966
10% Ha composite	32		9.42
15% Ha composite	31.73		11.795

Hydroxyapatite/chitosan powder was formed by grinding previously described hydroxyapatite/chitosan composites with a mortar and pestle. The original composites were broken into smaller pieces, about 5 mm in diameter, then ground in the mortar. As particles reached a uniform size, they were removed and replaced with larger pieces. The final powder was found to have diameter on the order of 100 μm using optical microscopy.

All components were then combined and dry mixed for at least 2 minutes. The mold was placed in the hot press, with a layer of polyimide film protecting the equipment from the part. The mold was filled evenly with the dry mixture of components and then overfilled by 2mm. The part was pre-compacted with a load of 20,000 lbs, then unloaded. The mold was overfilled again by 2mm.

The part was formed under a pressure of 17 MPa and a temperature of 195 °C. The part was elevated to the operating temperature of 195 °C over a period of 1 hour, then held at this temperature for 40 minutes and allowed to gradually cool under pressure over approximately 45 minutes. A constant pressure of 17 MPa was used during molding.

3.2 Material Characterization

After compression molding, all composite and neat polyethylene samples were investigated using optical and scanning electron microscopy. Images of both molding surfaces and fracture surfaces were taken.

Figures 2.1a and b show the surface of a neat polyethylene sample. The porosity of the sample can be seen. During molding, the individual particles of UHMWPE do not flow together; instead they bond together, while retaining individual morphology. Figure 3.1c, a polished cross section, further illustrates this point.

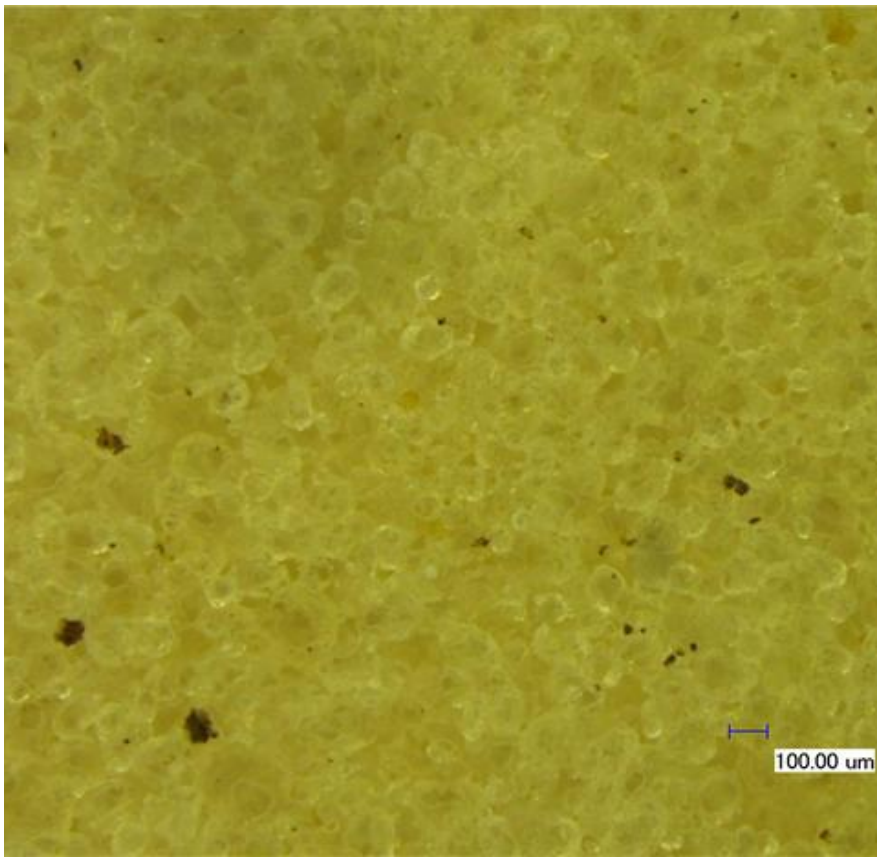

Figure 3.1a: Optical image of 100% UHMWPE surface. Individual particles of UHMWPE are visible

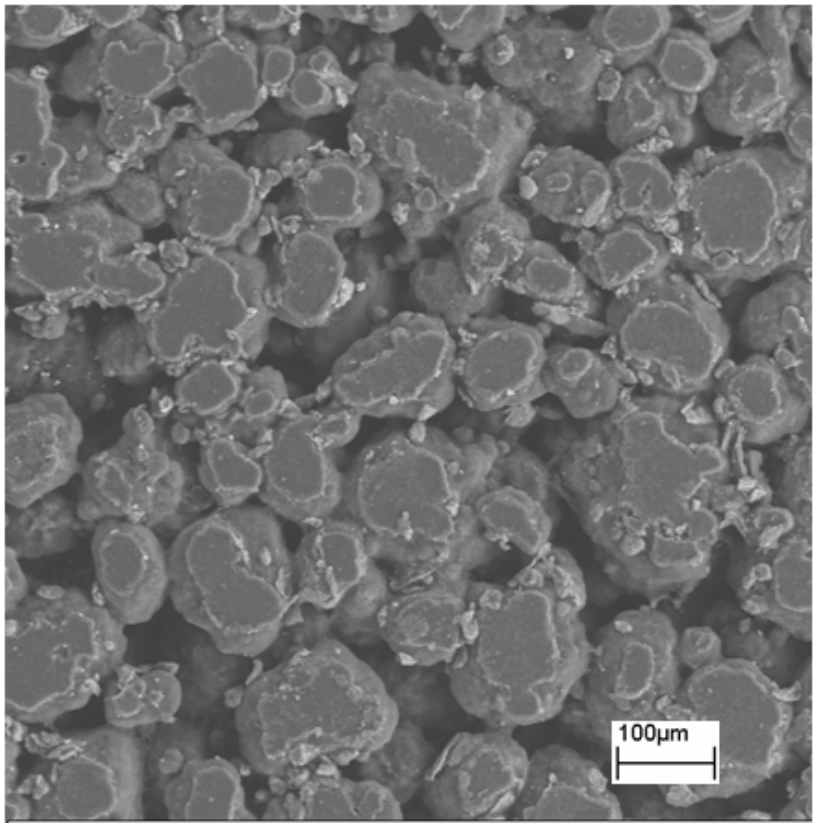

Figure 3.1b: SEM image of 100% UHMWPE molding surface

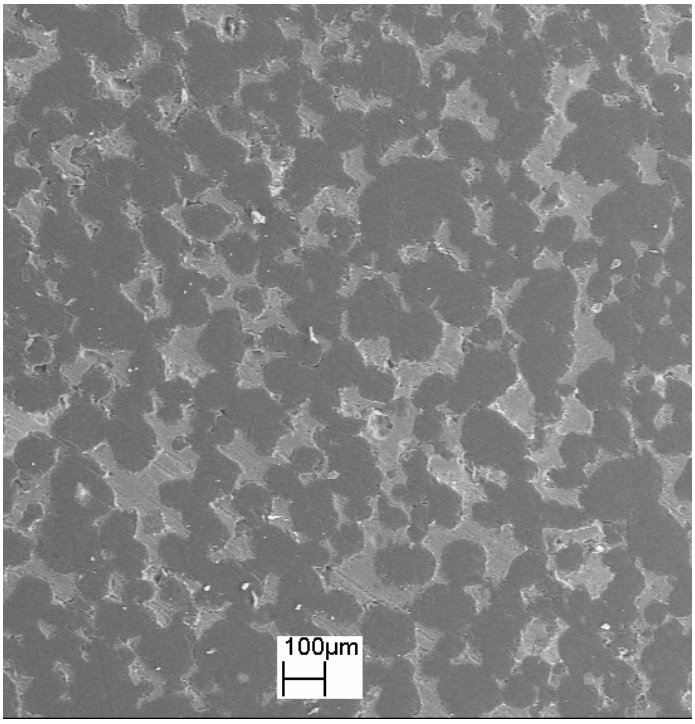

Figure 3.1c: SEM of 100% UHMWPE polished cross section

Figures 2.2a and b show the surface of a hydroxyapatite reinforced polyethylene. The images show the individual particles of hydroxyapatite molded between the particles of polyethylene. Dispersion of hydroxyapatite is good and the hydroxyapatite particles are largely undamaged.

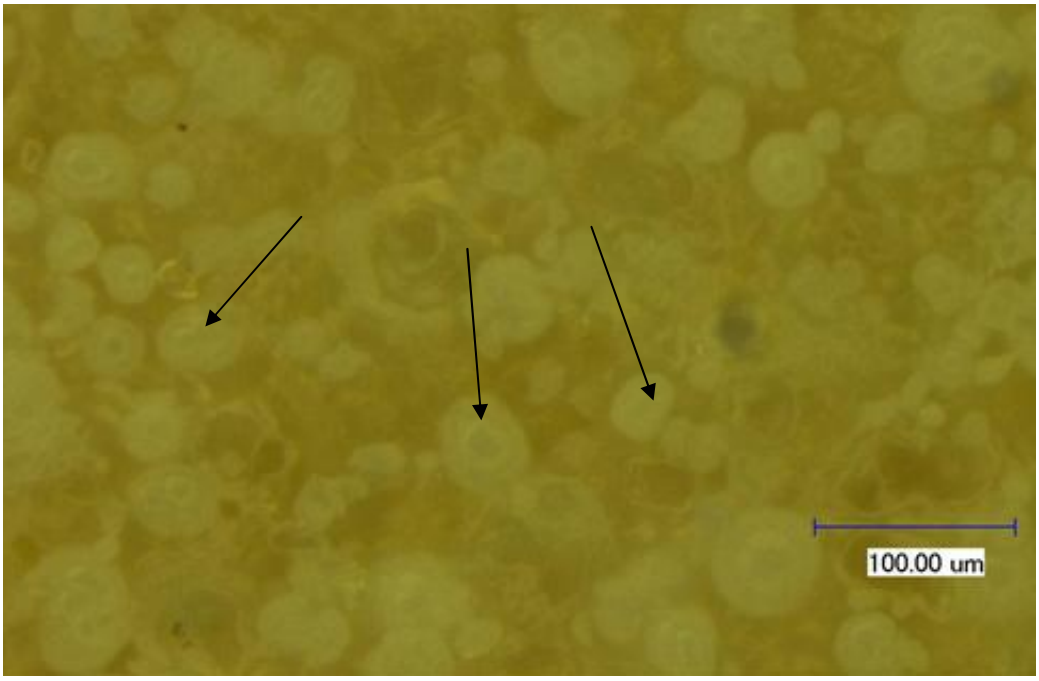

Figure 3.2a: Optical image of hydroxyapatite/UHMWPE sample. White, spherical hydroxyapatite particles are dispersed between UHMWPE particles. Arrows indicate hydroxyapatite particles.

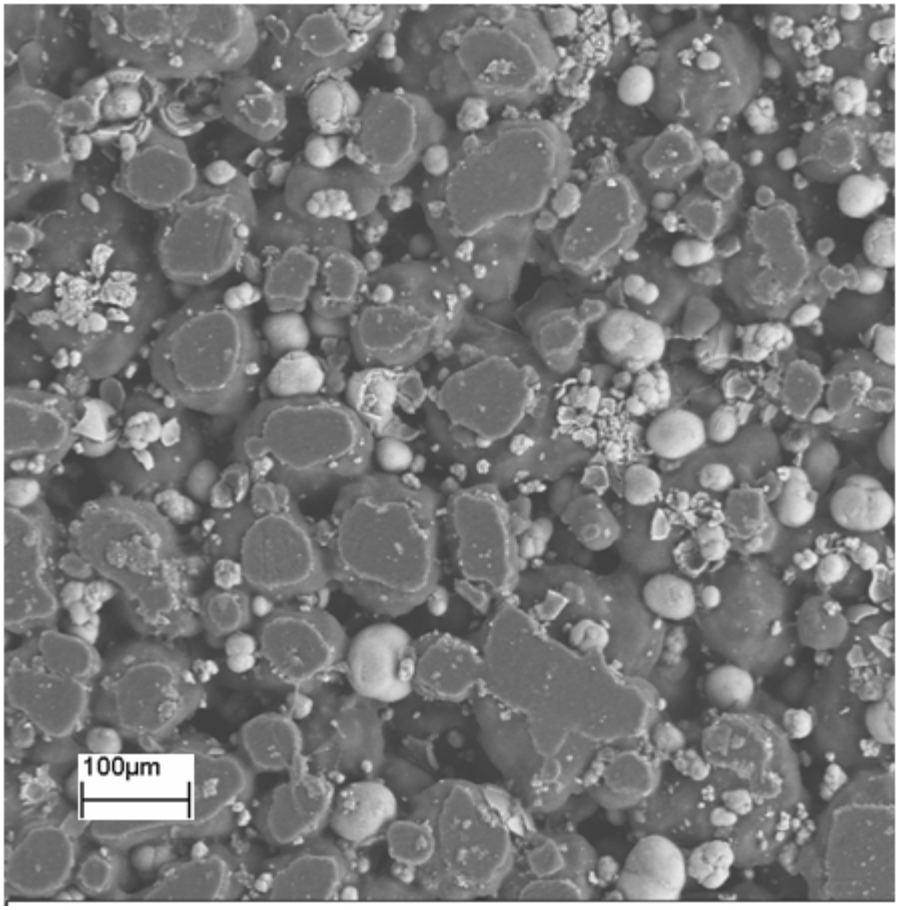

Figure 3.2b: SEM image of hydroxyapatite/UHMWPE sample. Spherical hydroxyapatite particles are dispersed between UHMWPE particles. Hydroxyapatite particles are undamaged.

Figures 2.3a and 3b show the surface of polyethylene reinforced with the chitosan/hydroxyapatite composite. Ground particles can be seen intermittently throughout the UHMWPE. The particles are similar to the ground chitosan/hydroxyapatite composite morphology with the exception of having changed to a brownish color. Heat from compression molding causes the malic acid/chitosan matrix to degrade. Simple testing by progressive heating indicates the malic acid has a degradation temperature below 140□C and the chitosan over 190□C.

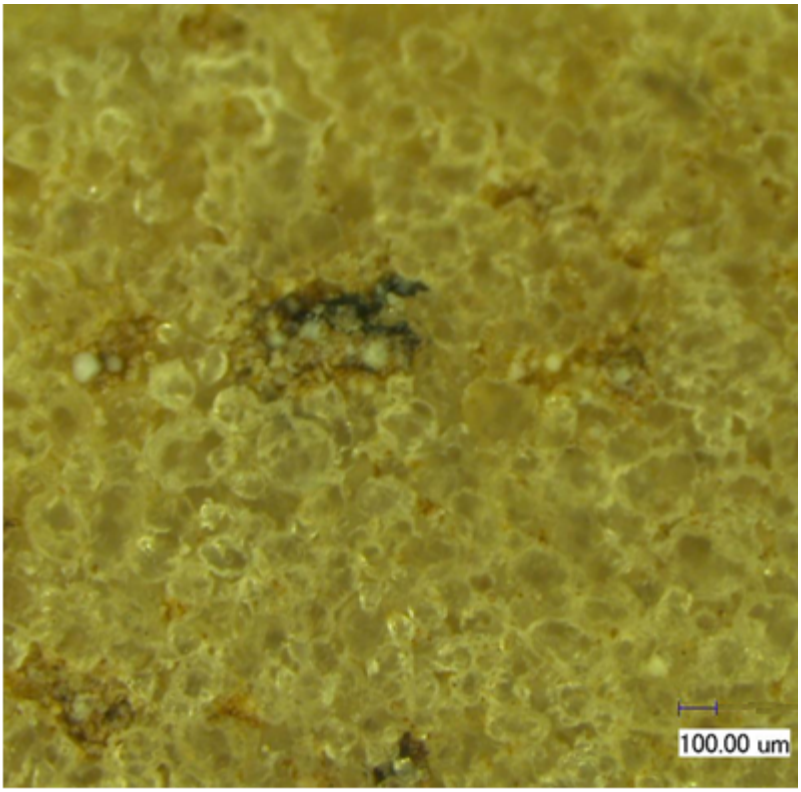

Figure 3.3a: Optical image of UHMWPE reinforced with chitosan/hydroxyapatite. Brown discoloration can be seen in the chitosan/hydroxyapatite composite.

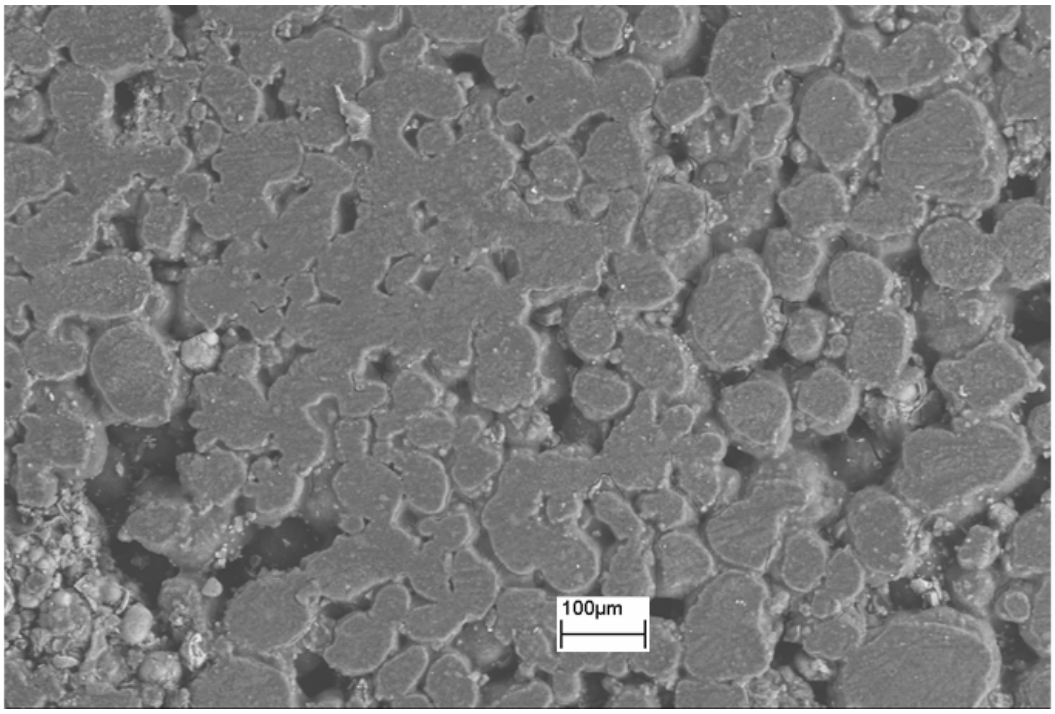

Figure 3.3b: SEM image of UHMWPE reinforced with chitosan/hydroxyapatite. Chitosan/hydroxyapatite particles have been broken during grinding and compression molding.

Figures 3.4a-c show the fracture surfaces of two composites. Figure 3.4a is reinforced with hydroxyapatite particles; Figure 3.4b is reinforced with chitosan/hydroxyapatite particles. The wear performance of the composite is influenced by the cohesive strength of the composite material. A region of interest for the cohesive strength is the interface between the hydroxyapatite reinforcement, the chitosan and the polyethylene. At the point of fracture (cohesive failure), Figures 3.4a and 4b show the interface between the hydroxyapatite and polyethylene. Both samples show dimples in the polyethylene particles where reinforcement particles were previously adhered to UHMWPE. The dimples on the hydroxyapatite reinforced sample are smooth and dark, implying a clean and easy fracture. The dimples on the chitosan/hydroxyapatite sample are frayed and light, implying a great deal of energy was necessary to cause fracture. This shows chitosan is useful in creating a stronger polyethylene/chitosan composite, and improving the cohesive strength.

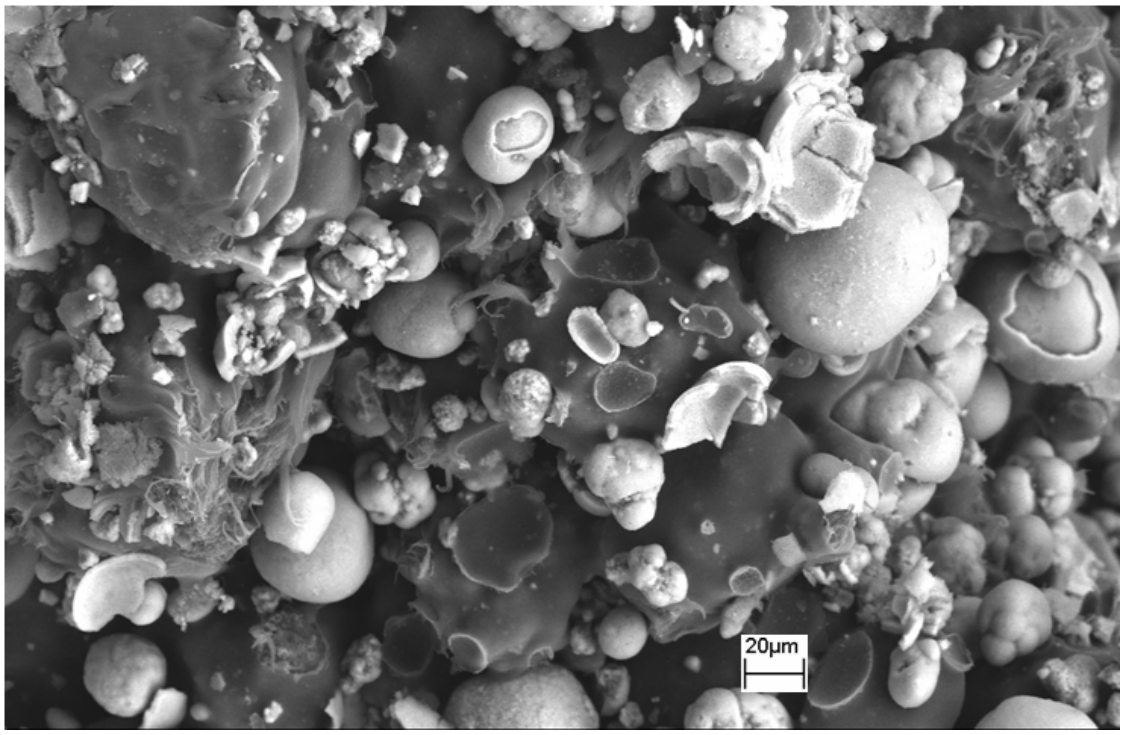

Figure 3.4a: SEM of fracture surface of UHMWPE reinforced with hydroxyapatite. Clean dimples at the point of fracture between hydroxyapatite and polyethylene indicate easy separation.

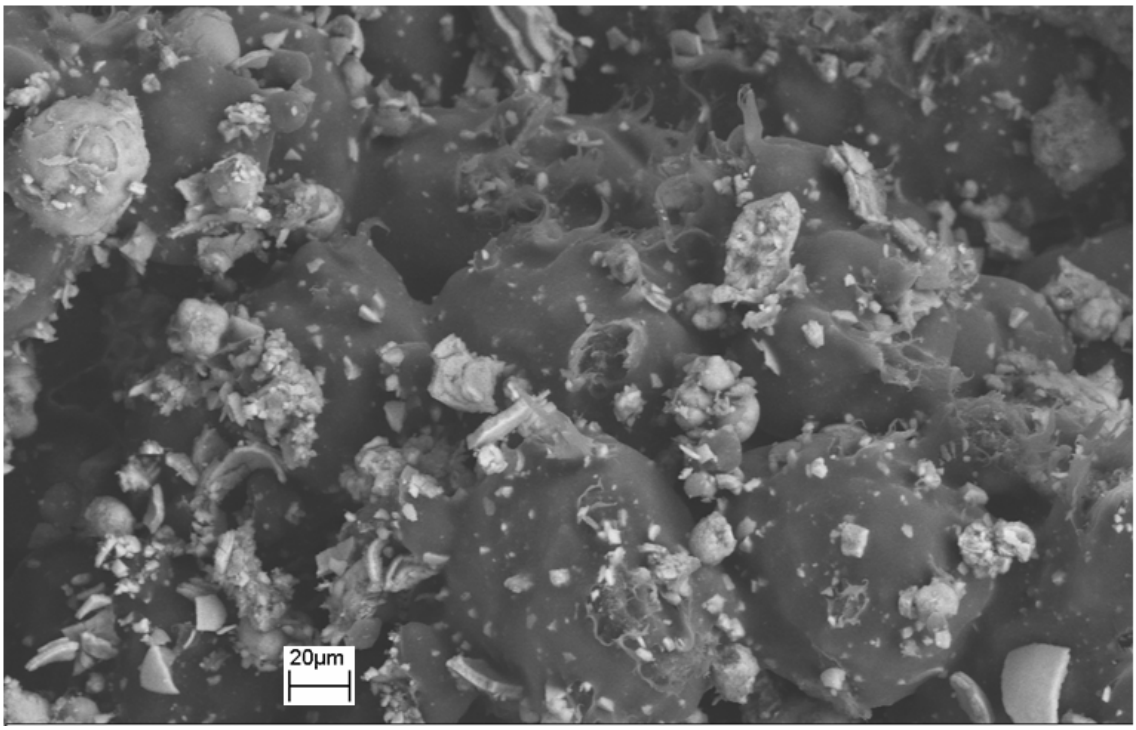

Figure 3.4b: SEM image of UHMWPE reinforced with chitosan/hydroxyapatite. Frayed dimples at the point of particle separation indicate higher energy necessary for fracture.

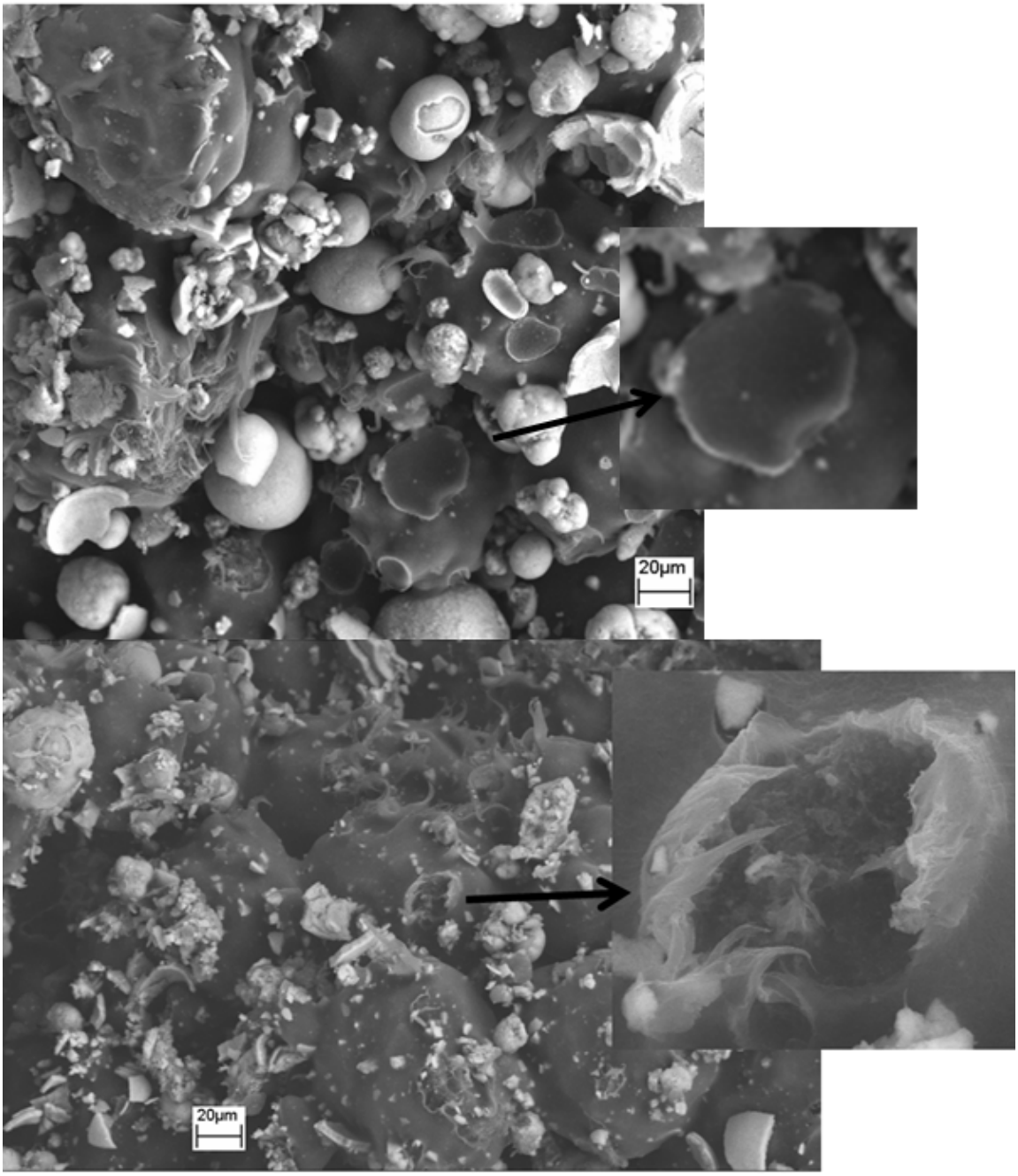

Figure 3.4c: A comparison of fracture surfaces from UHMWPE samples reinforced with hydroxyapatite and chitosan/hydroxyapatite. Chitosan/hydroxyapatite fracture surfaces appear more frayed and distorted than hydroxyapatite.

3.3 Tribotesting

A ball on flat tribotest is used to investigate the wear behavior of the UHMWPE/hydroxyapatite/chitosan composites. Parameters for testing which accurately link linear reciprocating wear to wear recorded in vivo have been well established[23-25]. Additionally, ASTM standard G133-95[26] provides test specifications for a ball on flat wear test. The testing procedure created was developed using these existing resources to best simulate joint wear using a CETR UMT-2 tribometer with a load range of 0.5-200 Newtons.

Ball on flat tribotesting may be better than a pin on disc test when investigating potential joint wear surfaces. Ball on flat testing introduces a fatigue component to the polymer not present in a pin on disc test. Also, the pressure distribution of a ball is nonlinear and more similar to a hip joint than the approximate constant pressure distribution in a pin on disc system.

Test samples were prepared by cutting a 50.8mm disc from sheets of compression molded UHMWPE/chitosan/hydroxyapatite samples, with the same processing conditions described earlier. An aluminum collar was glued to the disc to retain the lubricant during testing (Figure 3.5). Bovine Serum Albumin (BVA) was used as lubrication. Each sample was soaked in BVA for 42 hours prior to testing.

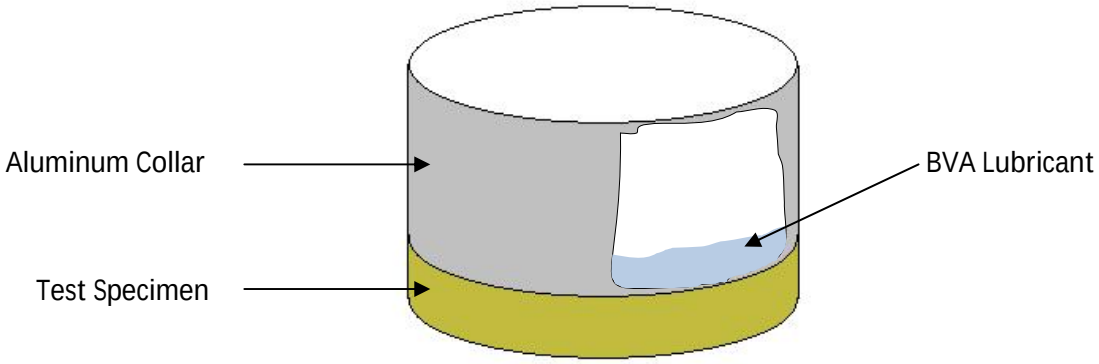

Figure 3.5: Cross section of composite test disc, collar and lubrication

All tests were performed on a CETR tribometer. Wear testing lasted 10 hour at a linear speed of 0.2 m/s. The counterface was a 6.35mm diameter 440C stainless steel ball with a specified surface roughness of 0.038 µm. A 1.5 N load was applied to the composite discs for a mean contact pressure of 32 MPa and a maximum contact pressure of 49 MPa, calculated by Hertzian contact analysis. For each test, the normal and friction forces were recorded at 10 Hz.

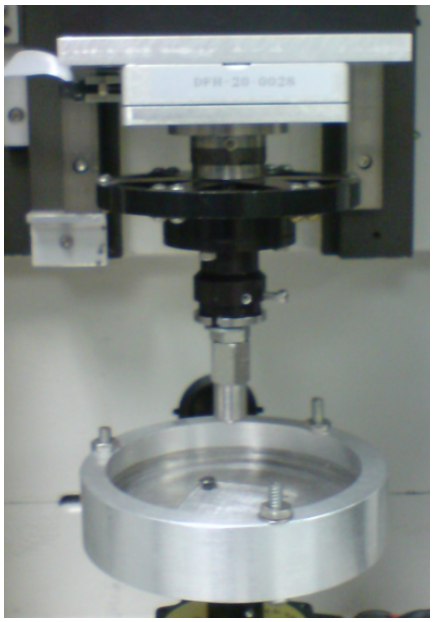

Figure 3.6: CETR tribometer

After wear testing, each sample was analyzed with a digital microscope (Keyence VHX500). Optical microscopy was used to measure wear track depth and width, as well as morphology. From the wear track width and depth, wear volume was calculated, even if the track cross sections had asymmetric edge heights.

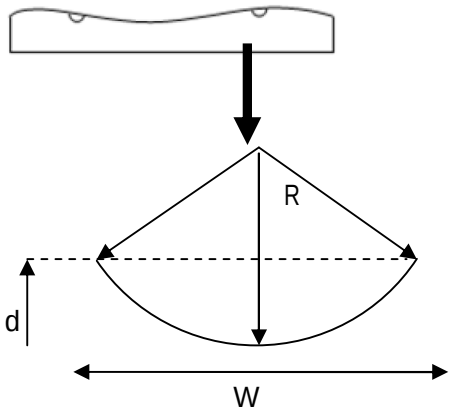

Figure 3.7: Cross section and dimensions of a wear track volume analysis. *R* is the ideal radius of curvature of the wear track, *d* is the depth of the wear track and *W* is the width of the wear track.

To calculate the wear volume, wear track dimensions were analyzed as found in Figure 3.7. The unknown value of the track curvature *R* must be found, from which wear volume can be found. From the geometry,

$$R^2 = \left(\frac{W}{2}\right)^2 + (R-d)^2 \qquad (3.1)$$

$$R^2 = \frac{W^2}{2} + R^2 - 2Rd + d^2 \qquad (3.2)$$

Simplifying,

$$R = \frac{W^2}{8d} + \frac{d}{2} \qquad (3.3)$$

The area of the cross section is given as:

$$\text{Area} = R^2 \arccos\left(\frac{R-d}{R}\right) - (R-x)\sqrt{2Rx - x^2} \tag{3.5}$$

where *d* is the average track depth and *W* is the track width. Cross sectional area is multiplied by the wear track circumference, which is determined from the center of the wear track, to calculate a value for wear volume lost.

3.4 Wear Track Characterization

After testing, samples were analyzed for tribological behavior. For each type of materials, both optical and SEM micrographs were taken of a wear track. These images can be seen in Figures 3.8-3.10.

Each material exhibited adhesive wear as expected in polymers. The images show how the individual particles of polyethylene have been plastically deformed and smeared across one another. Wear is worst at the center of the track and diminishes towards the edges. Surface deformation is highest in samples without reinforcement. The addition of reinforcement to polyethylene decreases plastic deformation due to the stiffening of the material.

Samples with hydroxyapatite reinforcement can be seen in Figures 3.9a and 3.9b. These wear tracks show a decrease in surface deformation when compared with neat polyethylene samples. Additionally, crushed hydroxyapatite particles are seen dispersed throughout the wear track. These pieces are what is left from reinforcement that was worked loose and crushed during wear testing.

Samples with chitosan/hydroxyapatite composite reinforcement can be seen in Figures 3.10a and 3.10b. The wear tracks shown in these images have particles of chitosan/hydroxyapatite reinforcement intact in the surface of the polyethylene. While there is still debris on the wear track likely originating from reinforcement, the intact particles which are not evident in the samples reinforced with only hydroxyapatite illustrates that reinforcement-polymer bonding is improved by the presence of chitosan.

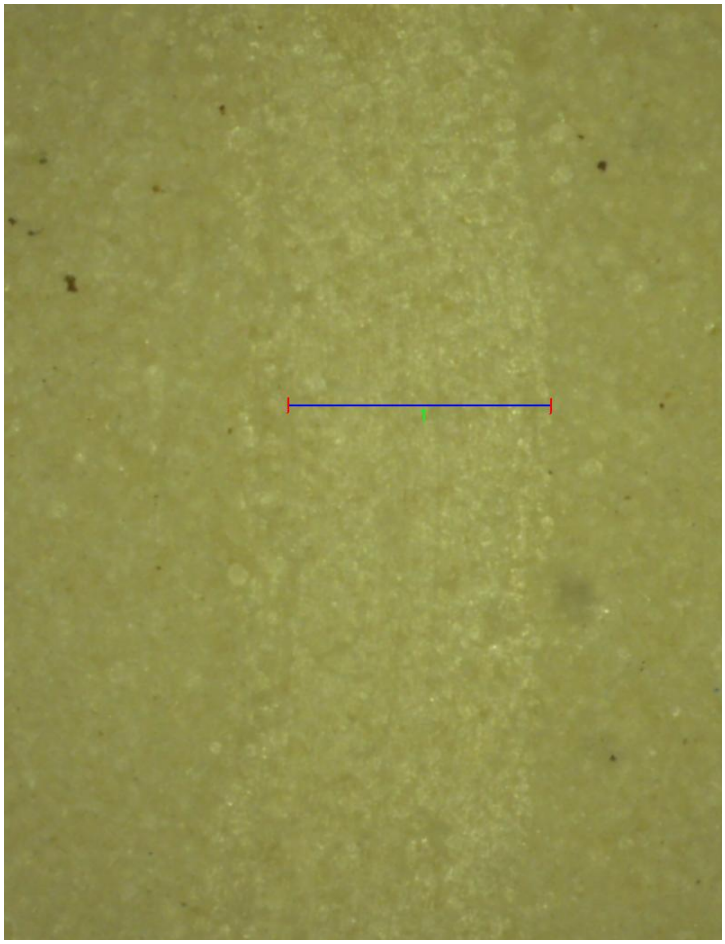

Figure 3.8a: Optical image of 100% UHMWPE wear track.

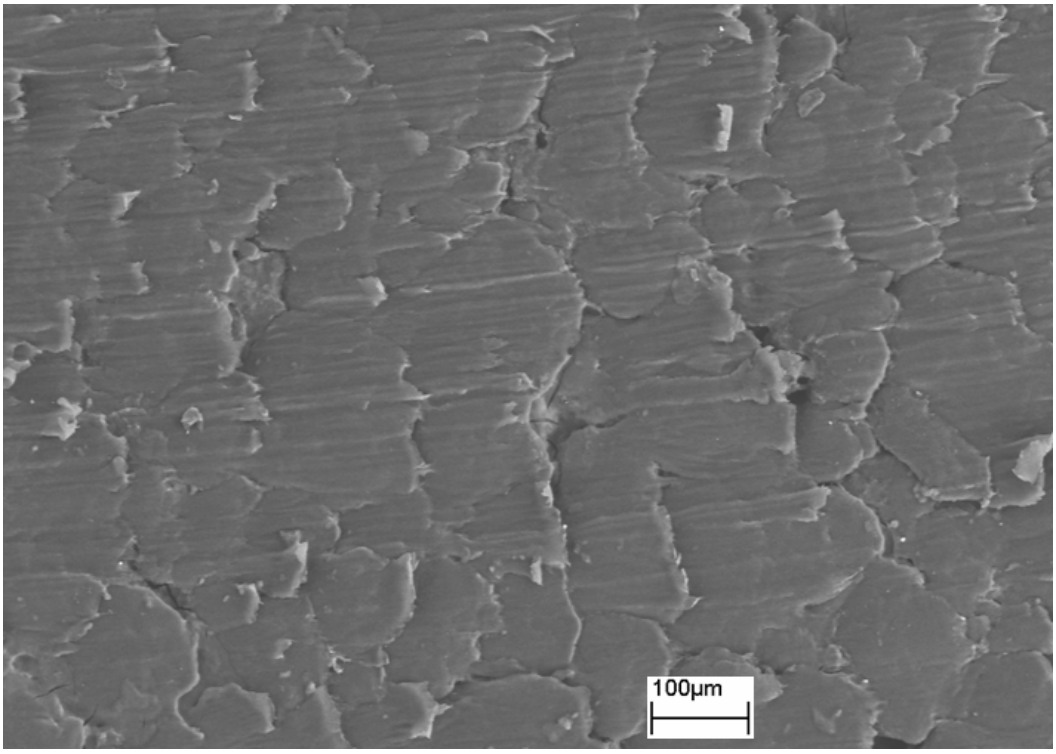

Figure 3.8b: SEM image of a 100% UHMWPE wear track. Considerable deformation has occurred due to adhesive wear.

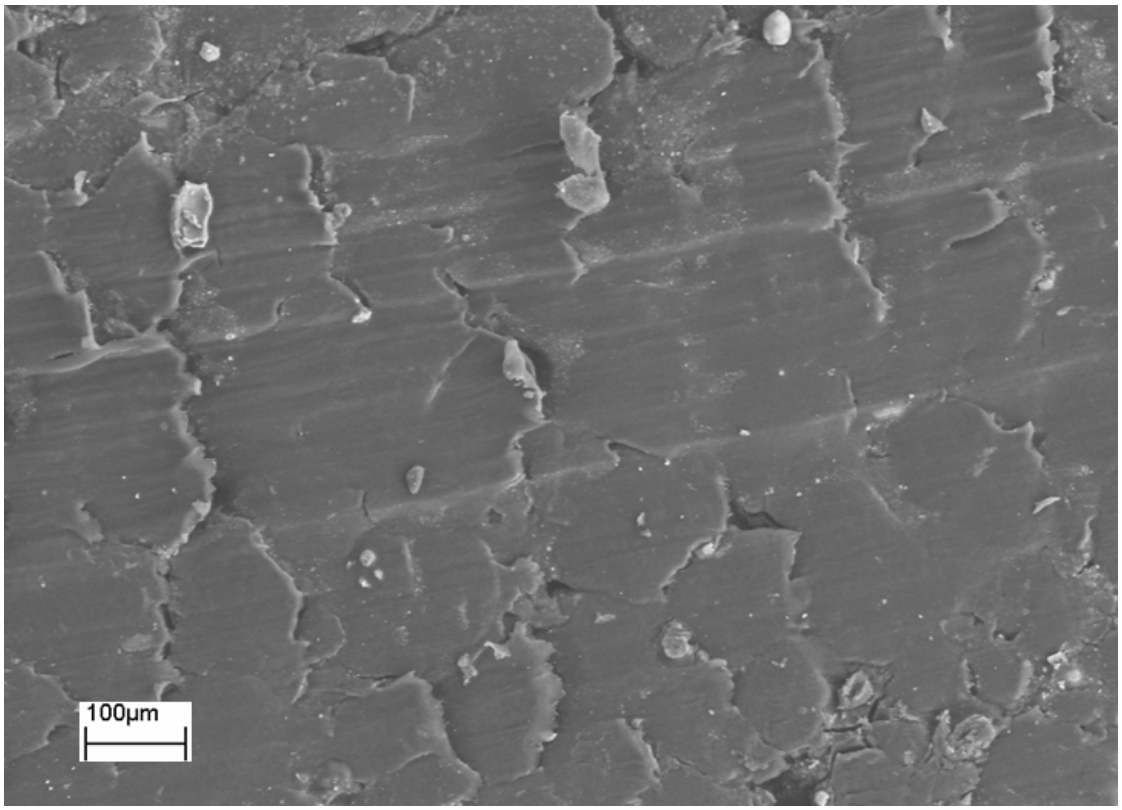

Figure 3.9a: Image of a 10% hydroxyapatite, 90% UHMWPE wear track. Debris in and around the wear track is high in calcium, likely from hydroxyapatite particles.

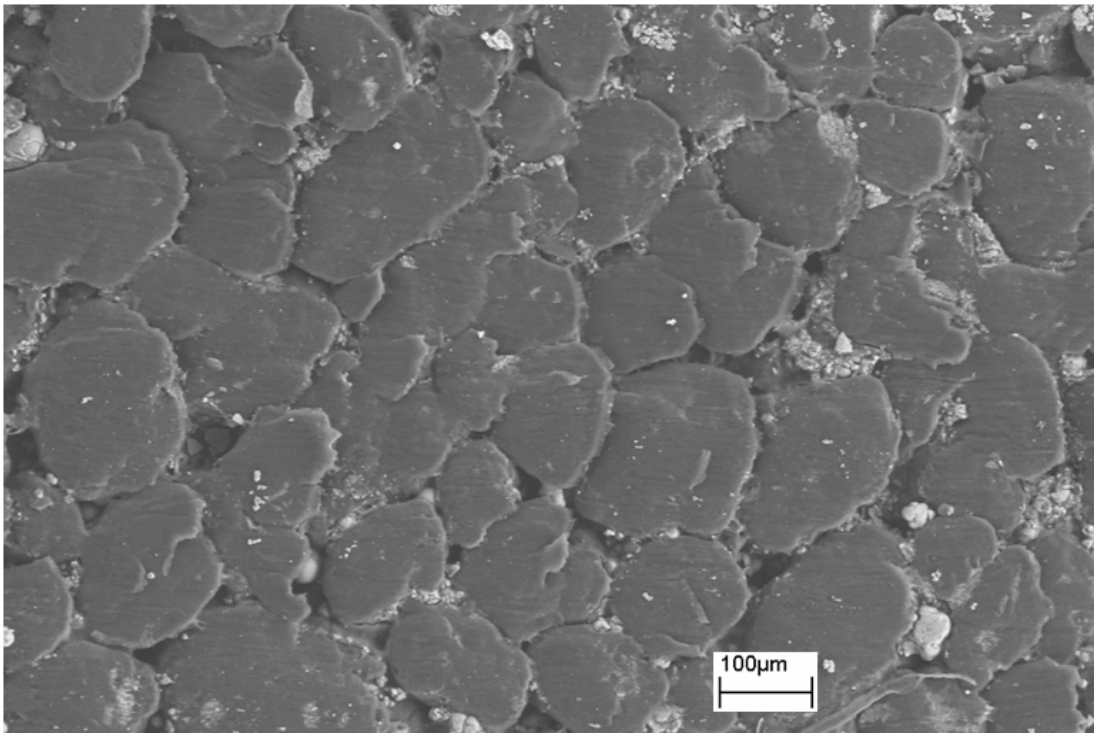

Figure 3.9b: Image of a 15% hydroxyapatite, 85% UHMWPE wear track. Surface deformation has decreased when compared to samples of lower reinforcement.

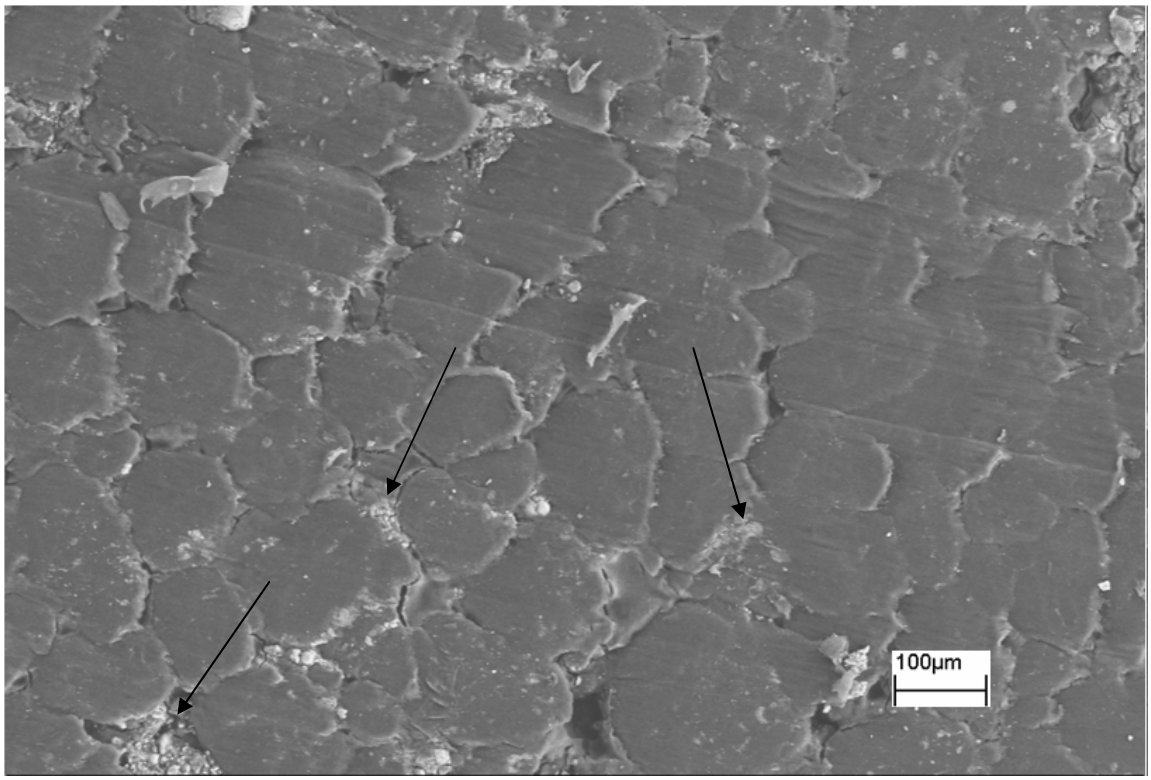

Figure 3.10a: Image of a 5% hydroxyapatite/chitosan, 95% UHMWPE wear track. Particles of intact hydroxyapatite/chitosan composite are visible in the wear track

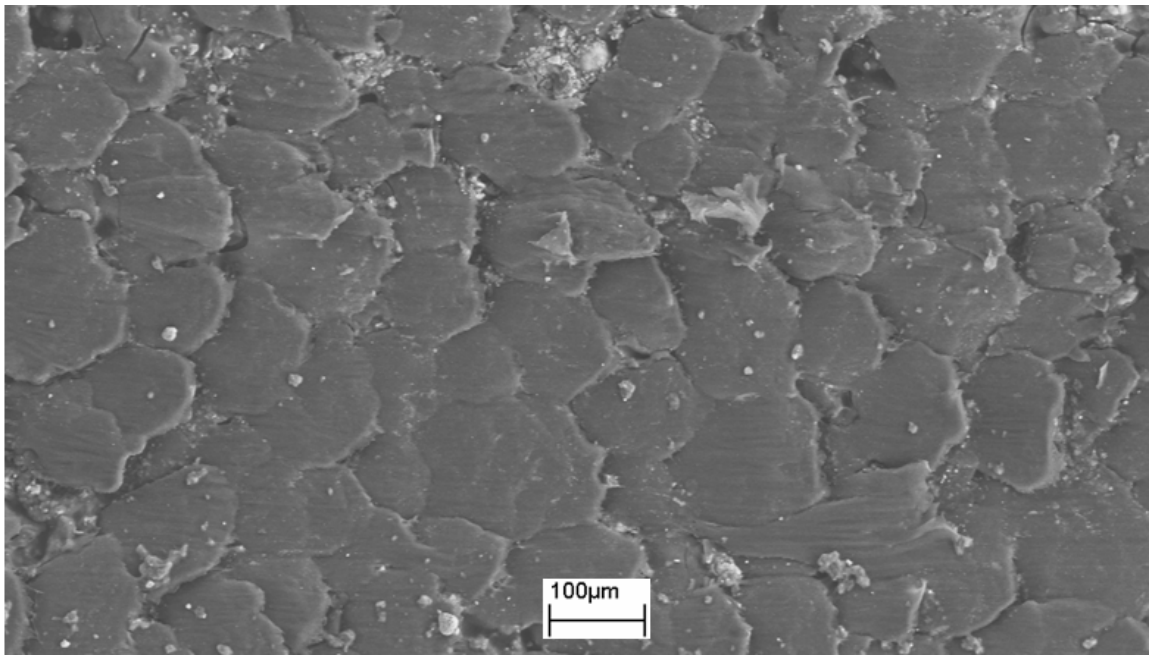

Figure 3.10b: Image of a 15% hydroxyapatite/chitosan, 85% UHMWPE wear track. Surface deformation has decreased when compared with samples of lower reinforcement.

3.5 Transfer Films

The ball bearings used as wear counterfaces were investigated for the existence of a transfer film. In polymer wear, a transfer film can influence the wear characteristics of a material[12]. From these tests, transfer films accumulated on counterfaces corresponding to reinforced samples, but were not present on counterfaces corresponding to samples of neat polyethylene.

Reinforcement may have the effect of increasing the adhesion of a transfer film to the ball. This increased adhesion may actually decrease wear rates. The built up transfer film reduces the wear of polymers by creating a constant wear surface for the activation of adhesive wear. In a sample where transfer films are not present, new material must be built up on each pass for relative motion to occur.

The composite samples, both with and without chitosan, developed transfer films on the counterfaces, seen in images 11 & 12. The polyethylene samples did not develop transfer films. In addition to the higher stiffness of composites, this may explain another mode by which reinforcement decreases wear.

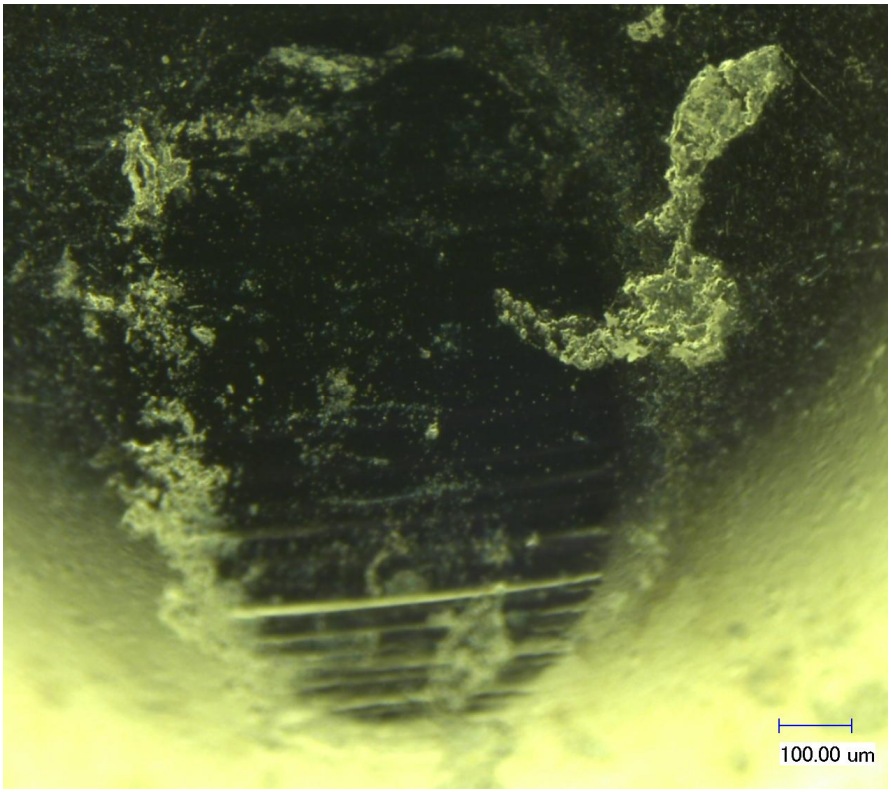

Figure 3.11: Optical image of transfer film on the wear counterface of a sample containing 10% hydroxyapatite and 90% UHMWPE.

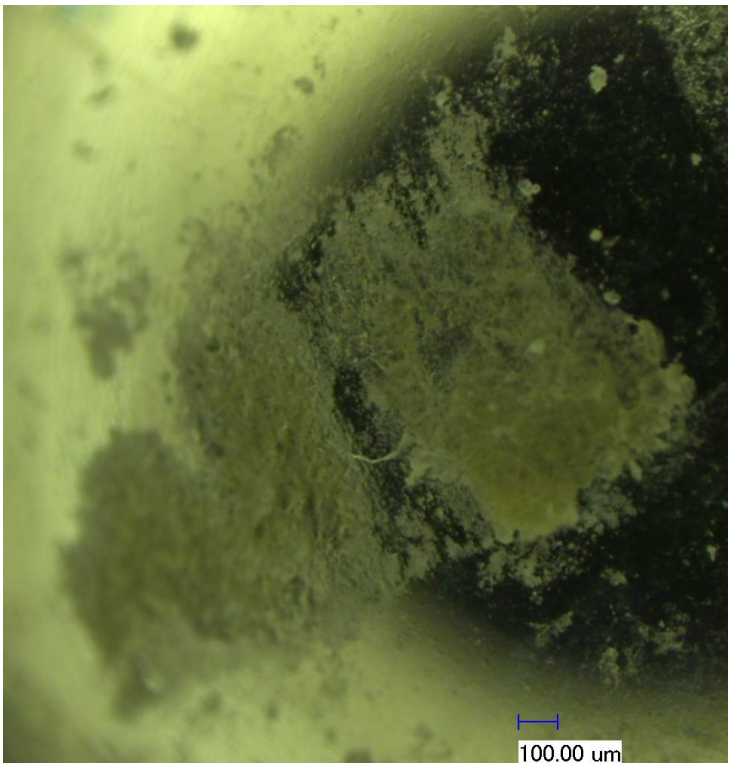

Figure 3.12: Transfer film on the wear counterface of a sample containing 10% chitosan/hydroxyapatite and 90% UHMWPE.

3.6 Wear Volume

Wear volume was calculated as explained earlier. Plots of the wear volume lost can be seen in Figures 3.13 – 15. Hydroxyapatite-reinforced polyethylene exhibited greater wear resistance than neat polyethylene. Chitosan/hydroxyapatite further increased wear resistance. Wear resistance increased from 0-5% reinforcement and again from 5-10% reinforcement, but decreased as more reinforcement was added. This critical point is due to large amounts of reinforcement reducing the toughness of the composite.

Increased wear resistance in these composites is due to three factors. Reinforcement of the polymer increases the stiffness of the material and the nominal area of contact at a given load. The reduced area of contact reduces the area on the sample where wear occurs and thus overall wear. Reinforcement also acts to break up the chain mechanisms which occur in polymer wear. Because UHMWPE is composed of long polymer chains, wear of a small area can cause damage a larger scale as the chains are pulled apart. The inclusion of reinforcement breaks up this transfer of material from the wear surface to the counterface. The last mechanism is the presence of a well adhered transfer film, as described above.

Table 3.2: Raw wear track dimensions as measured by optical microscopy. Depth is taken at deepest point in track.

	Average Depth (μm)	Average Width (μm)
PE	82.6	1632.7
PE	56.9	1509.8
PE	78.3	536.3
HaPE 1090	79.8	1411.3
HaPE 1090	11.2	948.8
HaPE 1090	14.7	899.5
HaPE 1585	56.8	483.8
HaPE 1585	51.2	566.8
HaPE 1585	26.8	438.3
ChHaPE 595	41.2	1174.0
ChHaPE 595	37.9	1084.4
ChHaPE 595	38.3	925.7
ChHaPE 1090	121.3	1724.6
ChHaPE 1090	19.9	562.8
ChHaPE 1090	7.9	439.6
ChHaPE 1585	20.0	463.2
ChHaPE 1585	47.9	1081.5
ChHaPE 1585	13.2	705.6

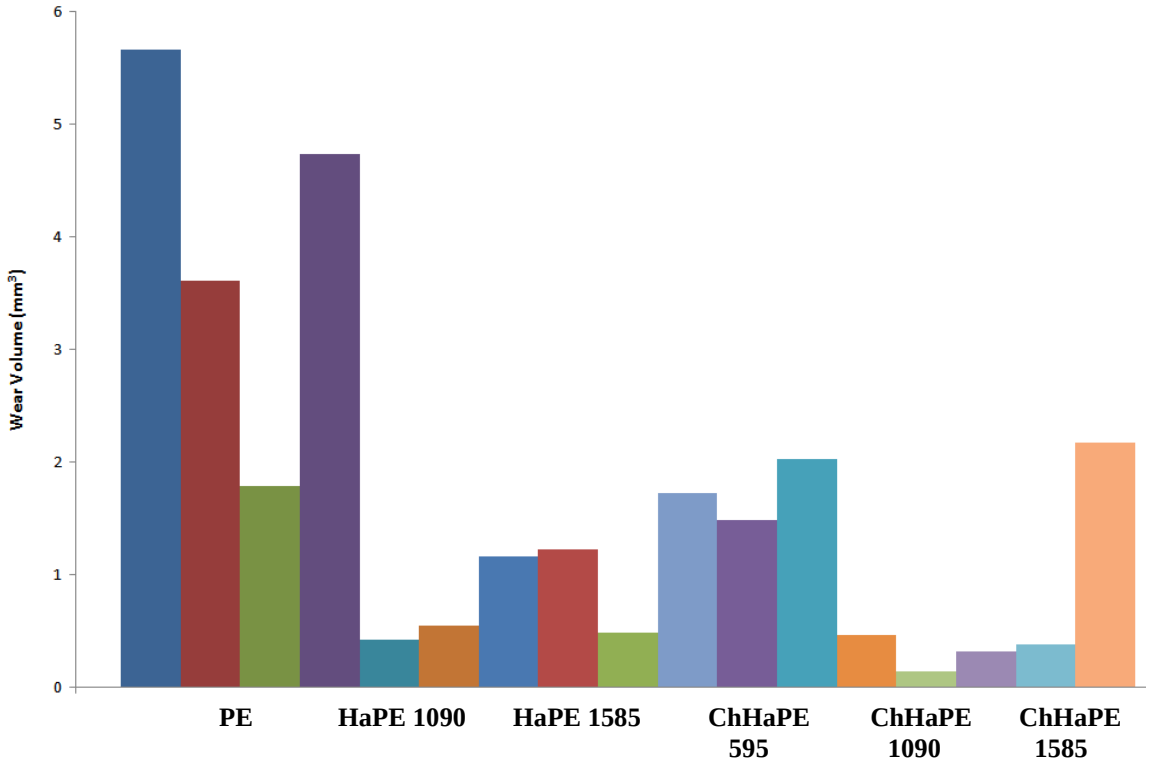

Figure 3.13: Wear volume lost during wear testing of individual samples

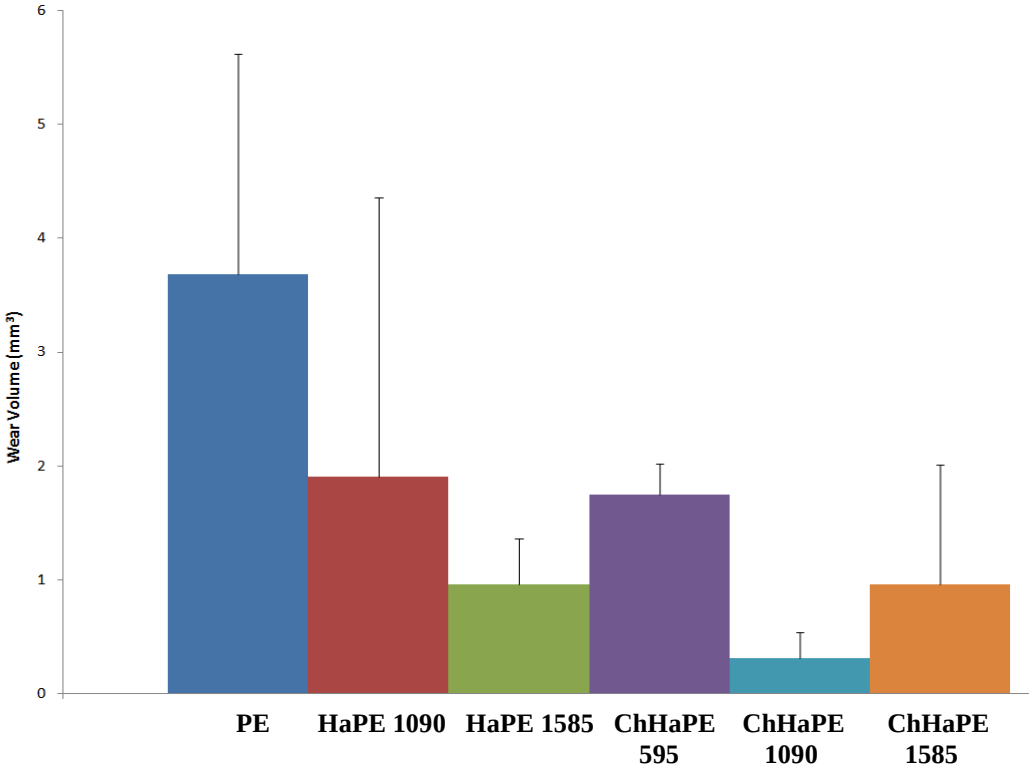

Figure 3.14: Wear volume lost by sample type. Hydroxyapatite reinforcement increases wear resistance. Chitosan/hydroxyapatite reinforcement further increases wear resistance. Each value is an average of three samples tested.

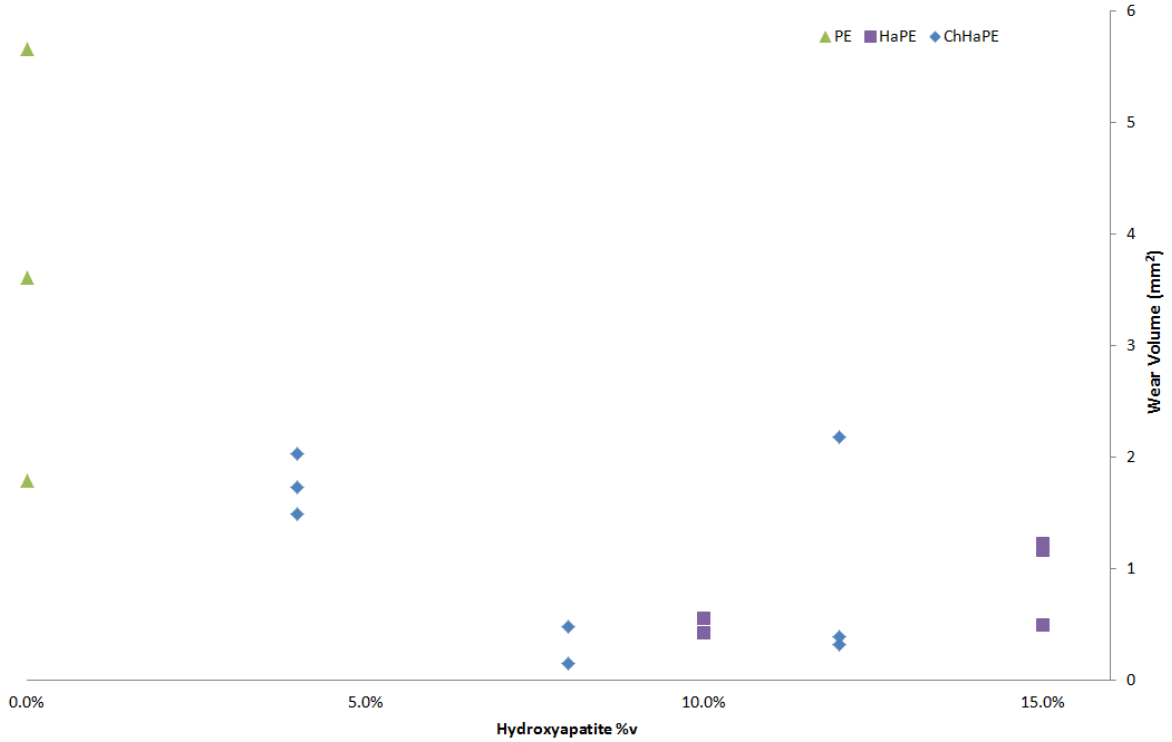

Figure 3.15: Wear volume lost vs. reinforcement loading. Optimum reinforcement loading appears to trend towards 10%.

3.6.1 Wear Coefficient

The Archard coefficient, *K*, is defined as[27]:

$$V = Kl\frac{W}{H}$$

Where *V* is wear volume, *l* is sliding distance, *W* is normal load and *H* is Vickers hardness. The Archard coefficient is an index of wear severity. In this test, Archard coefficient is dependant only on volume lost, as a constant sliding distance and load were used and a Vickers hardness of 6.7 was assumed for each material[28].

Table 3.3: Wear rates and Archard coefficients for different materials. Wear rate and Archard coefficient are higher in specimens of 100% UHMWPE and lowest in samples reinforce with 10% chitosan/hydroxyapatite composite.

Wear Rate (mm^3/km)	Archard Coefficient $x10^{-10}$
0.51	0.023
0.26	0.012
0.13	0.006
0.24	0.011
0.04	0.002
0.13	0.006

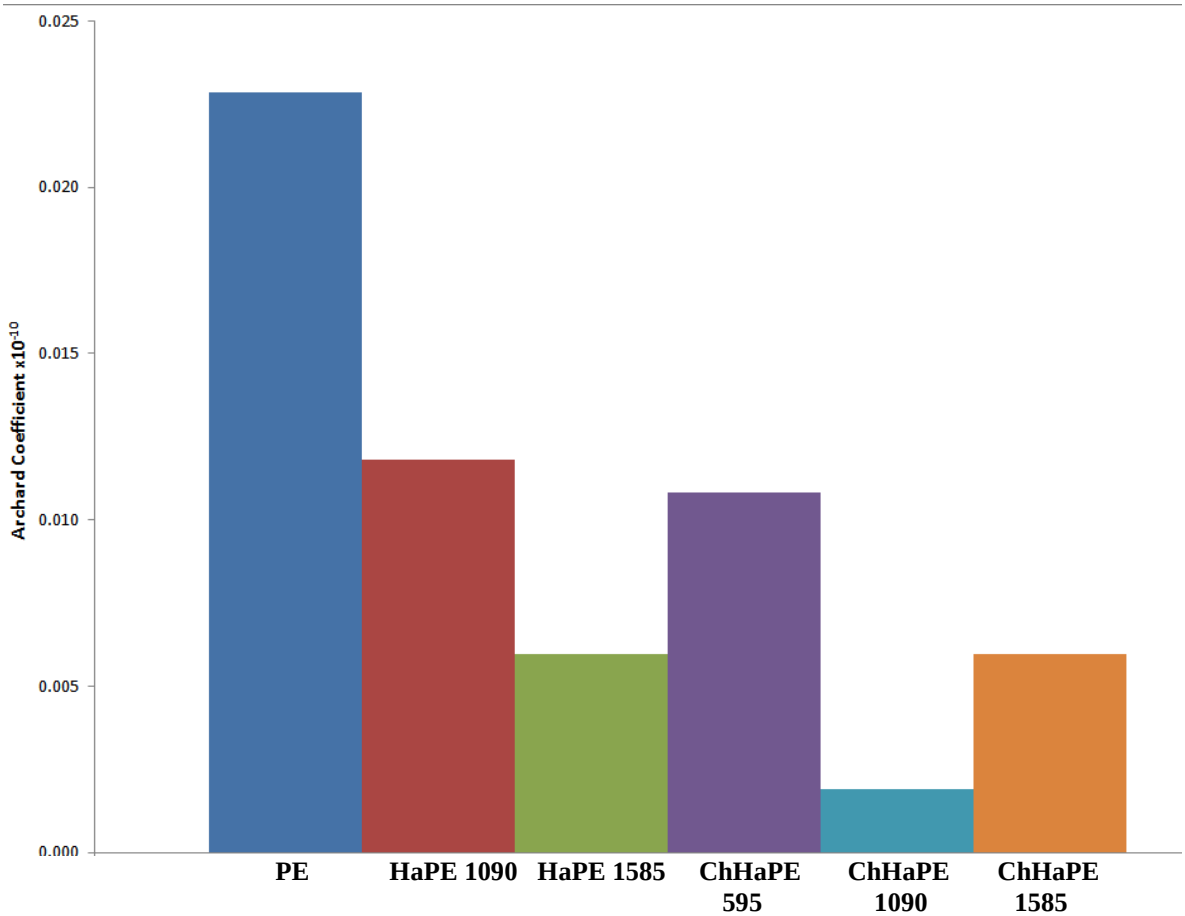

Figure 3.16: Archard coefficients (K) for different material types. Coefficients correlate directly with wear volume lost.

3.7 Friction

Readings for both normal and frictional loads were recorded and used to determine the coefficient of friction. An example of the recorded data can be seen in Figure 3.17. Data collected from each sample contained three distinct features: A high initial friction coefficient which decreased during wear in over the first three hours, a steady state value of friction coefficient, and at least one event, a sharp increase or decrease in friction coefficient. Events did not occur at the same time in each sample, so it is difficult to determine their origin. It is possible lubrication and re-lubrication of the samples with bovine serum caused the change in friction coefficient.

Both initial and steady state values were recorded for each wear test and can be seen in Figures 3.18 and 3.19. The values for friction coefficient are consistent and do not vary predictably between different samples or materials.

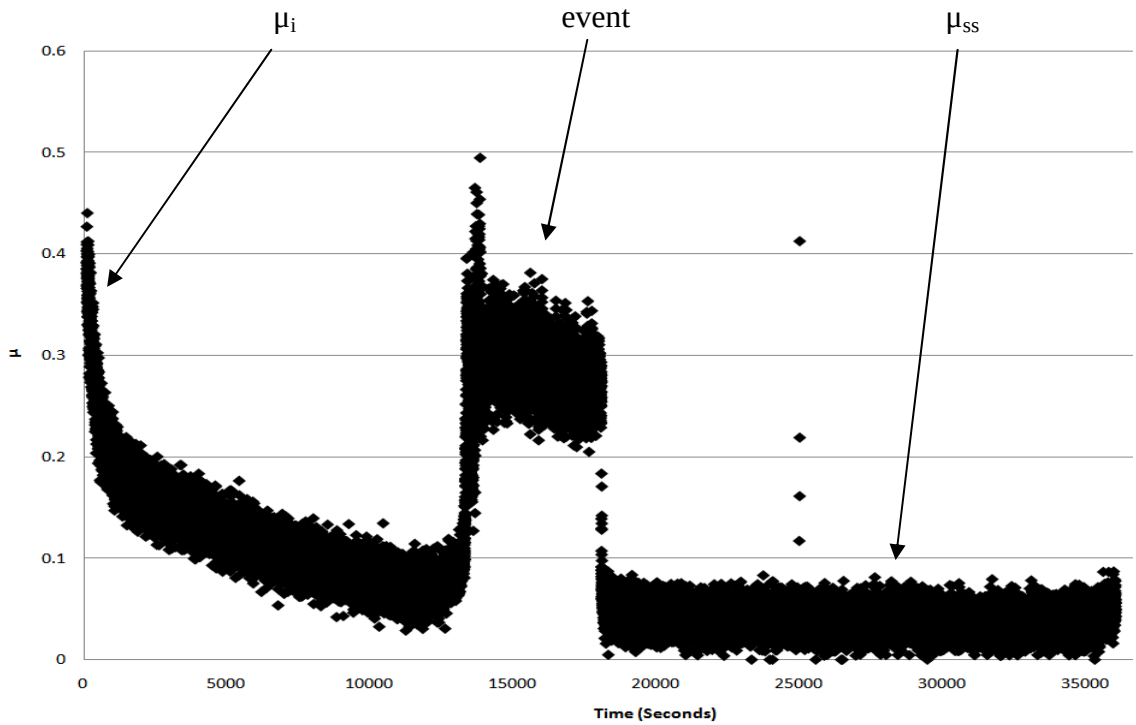

Figure 3.17: Coefficient of friction, μ, over a ten hour test. Friction is initially high, and then quickly wears in with events at 13000 and 25000 seconds.

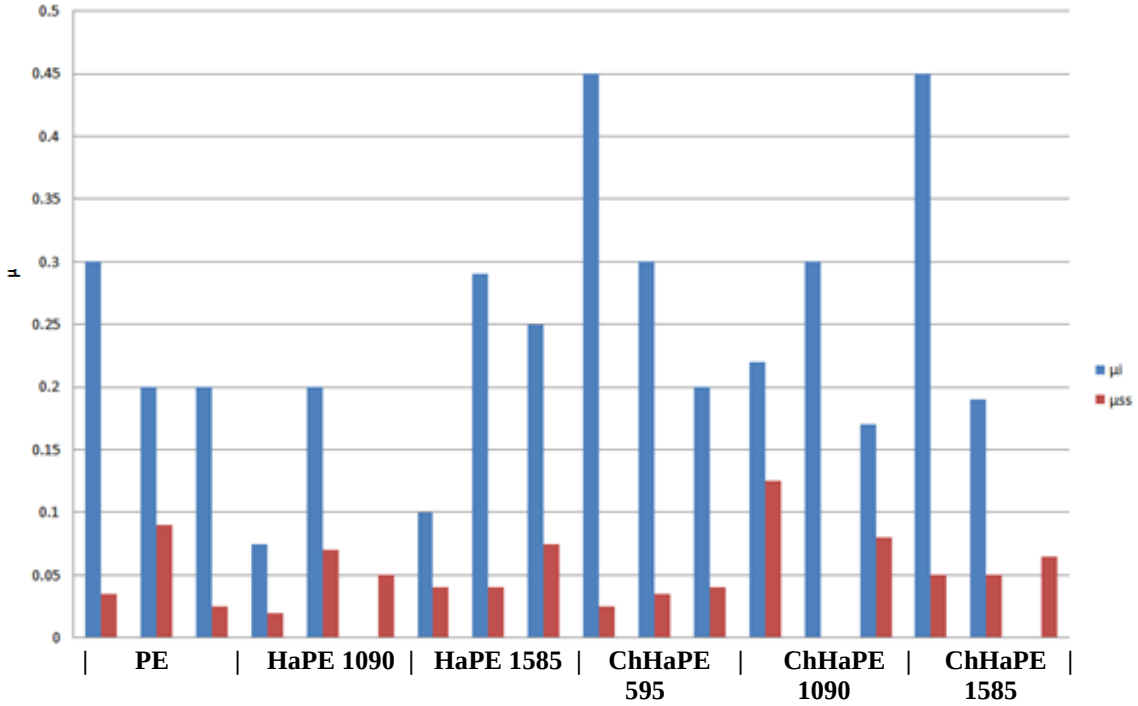

Figure 3.18: Data taken for initial and steady state friction from each sample. Both initial and steady state friction show little correlation.

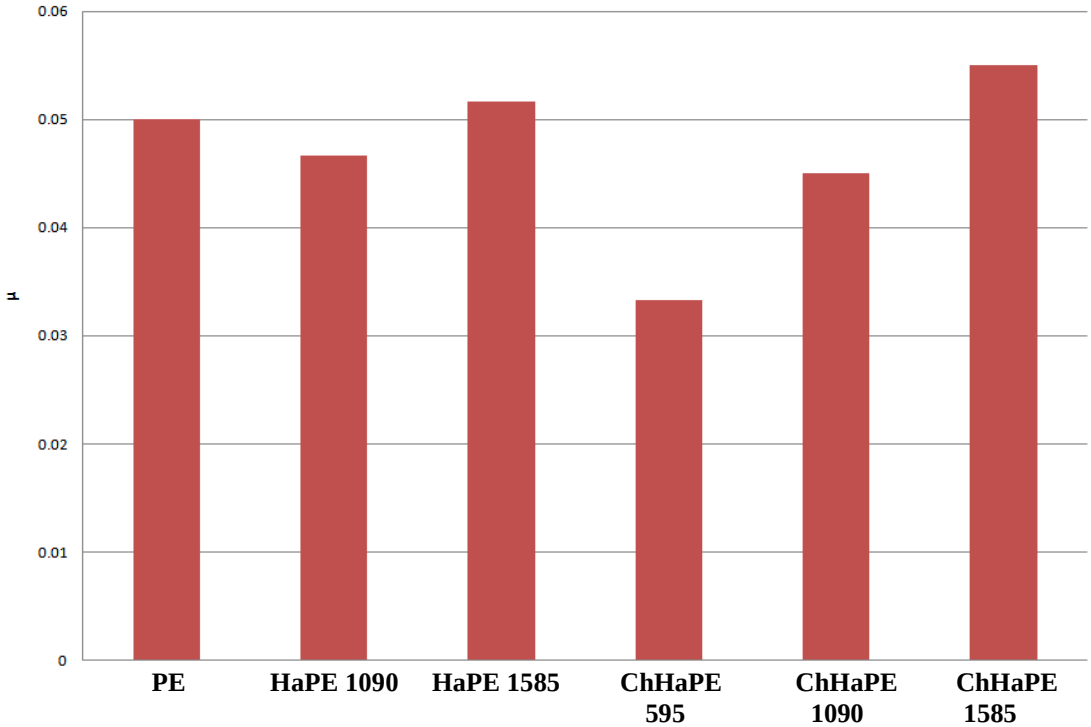

Figure 3.19: Steady state friction for each type of material. Steady state friction shows little correlation to material type.

Chapter 4
Conclusions

This work presents hydroxyapatite/chitosan and hydroxyapatite/chitosan/polyethylene particle reinforced composites which have been developed and characterized with emphasis on performance in orthopedic applications.

- Both chitosan/hydroxyapatite and hydroxyapatite/chitosan/polyethylene have been prepared with good reinforcement distribution. Optical and SEM micrographs indicate there is little clustering of reinforcement particles.
- Chitosan is shown to evenly coat and interact preferably with hydroxyapatite particles. SEM micrographs show chitosan integrates well as a matrix for hydroxyapatite reinforcement and evenly distributes among the particles. Fracture surface images shows the cohesive strength of chitosan/hydroxyapatite composites is higher than that of hydroxyapatite itself.
- Raman spectroscopy and TGA have shown a chemical interaction exists between hydroxyapatite and chitosan, indicating chitosan may improve previously poor bonding between hydroxyapatite and ultra high molecular weight polyethylene.
- AFAM testing shows chitosan coated hydroxyapatite particles have an elastic modulus of 10.7 GPa, between that of neat hydroxyapatite (70.1) and UHMWPE (1.7 GPa), signifying chitosan can be used a functional interlayer between the two.
- Ball on flat tribotesting has shown hydroxyapatite reinforcement decreases the wear rate of UHMWPE. Integration of a chitosan interlayer to hydroxyapatite

reinforcement further decreases the wear rate of UHMWPE. SEM images of polyethyelene composites show UHMWPE bonds better with chitosan/hydroxyapatite composites than neat hydroxyapatite particles do. SEM images also indicate chitosan/hydroxyapatite resists pullout in a wear test better than neat hydroxyapatite. A 10% Chitosan/HA – 90% UHMWPE composite was found to provide the best wear resistance.

Chapter 5
Recommendations

Recommendations for improvements in future research on these composites include:

- Design composite spheres of hydroxyapatite particles coated in chitosan as reinforcement for polyethylene composites. Rather than grinding previously formed composites, reinforcement should be designed for a particular filler size. Particle size and structural integrity of reinforcement could be engineered and controlled during materials fabrication.
- Better acid selection could improve material behavior. The use of malic acid contributed to discoloration and degradation of the chitosan/hydroxyapatite reinforcement during compression molding of polyethylene composites. While it didn't appear to effect wear performance of chitosan as an interlayer in polyethylene composites, alternative acids are available which are more resistant to thermal degradation.
- Use tension, compression and flexural testing to characterize materials. Additional mechanical testing could expose behavior of both the hydroxyapatite/chitosan composites and hydroxyapatite/chitosan/polyethylene composites
- Multidirectional wear testing. Multidirectional motion has been shown to better predict the wear performance of potential prosthetic wear materials[9]. A multidirectional pin on disk test or a joint simulator could further evaluate the potential of new polyethylene composites.

References

1. Bonfield, W., et al., *Hydroxyapatite reinforced polyethylene- a mechanically compatible implant material for bone-replacement.* Biomaterials, 1981. **2**(3): p. 185-186.

2. Khor, E. and L.Y. Lim, *Implantable applications of chitin and chitosan.* Biomaterials, 2003. **24**(13): p. 2339-2349.

3. Dowson, D., *A comparative study of the performance of metallic and ceramic femoral head components in total replacement hip joints.* Wear, 1995. **190**(2): p. 171-183.

4. Ito, M., *Invitro properties of a chitosan-bonded hydroxyapatite bone-filling paste.* Biomaterials, 1991. **12**(1): p. 41-45.

5. Sun, L.M., et al., *Fast setting calcium phosphate cement-chitosan composite: Mechanical properties and dissolution rates.* Journal of Biomaterials Applications, 2007. **21**(3): p. 299-315.

6. Xu, H.H.K. and C.G. Simon, *Fast setting calcium phosphate-chitosan scaffold: mechanical properties and biocompatibility.* Biomaterials, 2005. **26**(12): p. 1337-1348.

7. Sunny, M.C., P. Ramesh, and H.K. Varma, *Microstructured microspheres of hydroxyapatite bioceramic.* Journal of Materials Science-Materials in Medicine, 2002. **13**(7): p. 623-632.

8. Zhao, F., et al., *Preparation and histological evaluation of biomimetic three-dimensional hydroxyapatite/chitosan-gelatin network composite scaffolds.* Biomaterials, 2002. **23**(15): p. 3227-3234.

9. Wang, A., et al., *The significance of nonlinear motion in the wear screening of orthopaedic implant materials.* Journal of Testing and Evaluation, 1997. **25**(2): p. 239-245.

10. Isaac, G.H., et al., *A tribological study of retrieved hip prostheses.* Clinical Orthopaedics and Related Research, 1992(276): p. 115-125.

11. Elfick, A.P.D., et al., *Wear in retrieved acetabular components - Effect of femoral head radius and patient parameters.* Journal of Arthroplasty, 1998. **13**(3): p. 291-295.

12. Briscoe, B.J., A.K. Pogosian, and D. Tabor, *Friction and wear of high-density polyethylene- action of lead oxide and copper oxide fillers.* Wear, 1974. **27**(1): p. 19-34.

13. Zhao, Q. and S. Bahadur, *The mechanism of filler action and the criterion of filler selection for reducing wear.* Wear, 1999. **225**: p. 660-668.

14. Zhao, Q. and S. Bahadur, *A study of the modification of the friction and wear behavior of polyphenylene sulfide by particulate Ag2S and PbTe fillers.* Wear, 1998. **217**(1): p. 62-72.

15. Wang, M., D. Porter, and W. Bonfield, *Processing characterization, and evaluation of hydroxyapatite reinforced polyethylene composites.* British Ceramic Transactions, 1994. **93**(3): p. 91-95.

16. Wang, M., M. Chandrasekaran, and W. Bonfield, *Friction and wear of hydroxyapatite reinforced high density polyethylene against the stainless steel counterface.* Journal of Materials Science-Materials in Medicine, 2002. **13**(6): p. 607-611.

17. Chowdhury, S.K.R., et al., *Wear characteristic and biocompatibility of some polymer composite acetabular cups.* Wear, 2004. **256**(11-12): p. 1026-1036.

18. Chowdhury, S.K.R., et al., *Wear characteristic and biocompatibility of some hydroxyapatite-collagen composite acetabular cups.* Wear, 2007. **262**(11-12): p. 1387-1398.

19. Gao, P. and M.R. Mackley, *The structure and rheology of molten ultra-high-molecular-mass polyethylene.* Polymer, 1994. **35**(24): p. 5210-5216.

20. Fang, L.M., Y. Leng, and P. Gao, *Processing and mechanical properties of HA/UHMWPE nanocomposites.* Biomaterials, 2006. **27**(20): p. 3701-3707.

21. Zhao, W., R.P. Singh, and C.S. Korach, *Effects of environmental degradation on near-fiber nanomechanical properties of carbon fiber epoxy composites.* Composites Part a-Applied Science and Manufacturing, 2009. **40**(5): p. 675-678.

22. Karuppiah, K.S.K., et al., *Friction and wear behavior of ultra-high molecular weight polyethylene as a function of polymer crystallinity.* Acta Biomaterialia, 2008. **4**(5): p. 1401-1410.

23. Atkinson, J.R., et al., *Laboratory wear tests and clinical observations of the penetration of femoral heads into acetabular cups in total replacement hip joints .2. a microscopical study of the surfaces of charnley polyethylene acetabular sockets.* Wear, 1985. **104**(3): p. 217-224.

24. Cooper, J.R., D. Dowson, and J. Fisher, *Birefringent studies of polyethylene wear specimens and acetabular cups.* Wear, 1991. **151**(2): p. 391-402.

25. Cooper, J.R., D. Dowson, and J. Fisher, *Macroscopic and microscopic wear mechanisms in ultra-high-molecular-weight polyethylene.* Wear, 1993. **162**: p. 378-384.

26. Annual Book of ASTM Standards, *Standard Test Method for Linearly Reciprocating Ball-on-Falt Sliding Wear G133-95*. American Society for Testing and Materials International, 1992. p. 558-566.

27. Stachowiak, G.W.B., A. W., *Engineering Tribology*. 2005, Burlington MA: Butterworth-Heinemann.

28. Kusaba, A., et al., *In vivo change of elastic property in polyethylene acetabular components.* Modern Rheumatology, 2008. **18**(2): p. 140-145.

29. Hydroxyapatite MSDS No. 14608 [Online]; Sigma-Aldrich: St. Louis, MO. April 01, 2008 http://www.msds.sunysb.edu (accessed June 11, 2009)

30. Chitosan MSDS No. 14605 [Online]; Sigma-Aldrich: St. Louis, MO. April 11, 2008 http://www.msds.sunysb.edu (accessed June 11, 2009)

31. Malic Acid MSDS No. 14606 [Online]; Sigma-Aldrich: St. Louis, MO. Jan. 1, 2006 http://www.msds.sunysb.edu (accessed June 11, 2009)

32. Polyethylene MSDS No. 14607 [Online]; Sigma-Aldrich: St. Louis, MO. April 11, 2008 http://www.msds.sunysb.edu (accessed June 11, 2009)